nature nanotechnology

SUPPLEMENTARY INFORMATION

https://doi.org/10.1038/s41565-019-0395-0

In the format provided by the authors and unedited.

Bright sub-20-nm cathodoluminescent nanoprobes for electron microscopy

Maxim B. Prigozhin[1,15], Peter C. Maurer[1,15], Alexandra M. Courtis[2], Nian Liu[3,12], Michael D. Wisser[3], Chris Siefe[3], Bining Tian[4], Emory Chan[4], Guosheng Song[5,13], Stefan Fischer[3], Shaul Aloni[4], D. Frank Ogletree[4], Edward S. Barnard[4], Lydia-Marie Joubert[6,14], Jianghong Rao[5], A. Paul Alivisatos[2,7,8,9], Roger M. Macfarlane[10], Bruce E. Cohen[4], Yi Cui[3], Jennifer A. Dionne[3] and Steven Chu[1,11]*

[1]Department of Physics, Stanford University, Stanford, CA, USA. [2]Department of Chemistry, University of California at Berkeley, Berkeley, CA, USA. [3]Department of Materials Science and Engineering, Stanford University, Stanford, CA, USA. [4]Molecular Foundry, Lawrence Berkeley National Laboratory, Berkeley, CA, USA. [5]Department of Radiology, Stanford University, Stanford, CA, USA. [6]CSIF Beckman Center, Stanford University, Stanford, CA, USA. [7]Materials Sciences Division, Lawrence Berkeley National Laboratory, Berkeley, CA, USA. [8]Department of Materials Science and Engineering, University of California, Berkeley, CA, USA. [9]Kavli Energy NanoScience Institute, Berkeley, CA, USA. [10]IBM Research – Almaden, San Jose, CA, USA. [11]Department of Molecular and Cellular Physiology, Stanford University, Stanford, CA, USA. [12]Present address: School of Chemical and Biomolecular Engineering, Georgia Institute of Technology, Atlanta, GA, USA. [13]Present address: State Key Laboratory of Chemo/Biosensing and Chemometrics, College of Chemistry and Chemical Engineering, Hunan University, Changsha, China. [14]Present address: EM Unit, Central Analytical Facilities, Stellenbosch University, Stellenbosch, South Africa. [15]These authors contributed equally: Maxim B. Prigozhin and Peter C. Maurer. *e-mail: schu@stanford.edu

Bright sub-20 nm cathodoluminescent nanoprobes for electron microscopy

Maxim B. Prigozhin[#], Peter C. Maurer[#], Alexandra M. Courtis, Nian Liu, Michael D. Wisser, Christian Siefe, Bining Tian, Emory Chan, Guosheng Song, Stefan Fischer, Shaul Aloni, D. Frank Ogletree, Edward S. Barnard, Lydia-Marie Joubert, Jianghong Rao, A. Paul Alivisatos, Roger M. Macfarlane, Bruce E. Cohen, Yi Cui, Jennifer A. Dionne, Steven Chu*

Supplementary Information

Nanoparticle synthesis and characterization

The work described here addresses the development of small and bright nanoprobes for cathodoluminescence microscopy. To this end, a series of $NaGdF_4$ and $NaYF_4$ nanoparticles were synthesized. The nanoparticle synthesis protocol was based on previous reports[1–4].

Materials:

Oleic acid (Sigma-Aldrich, Cat# 364525-25ML, 90%, technical grade), 1-octadecene (Sigma-Aldrich, Cat# O806-1L, 90%, technical grade), rare-earth chlorides [cerium trichloride heptahydrate (Sigma-Aldrich, Cat# 202983-10G, 99.999%), praseodymium trichloride hydrate (Sigma-Aldrich, Cat# 205141-10G, 99.9%), neodymium trichloride hexahydrate (Sigma-Aldrich, Cat# 289183-25G, 99.9%), samarium trichloride hexahydrate (Sigma-Aldrich, Cat# 204277-5G, >99.99%), europium trichloride hexahydrate (Sigma-Aldrich, Cat# 212881-5G, 99.9%), gadolinium trichloride hexahydrate (Sigma-Aldrich, Cat# 203289-5G, 99.999%), terbium trichloride hexahydrate (Sigma-Aldrich, Cat# 212903-5G, 99.9%), dysprosium trichloride hexahydrate (Sigma-Aldrich, Cat# 203173-10G, >99.99%), holmium trichloride hexahydrate (Sigma-Aldrich, Cat# 289213-5G, 99.9%), erbium trichloride hexahydrate (Sigma-Aldrich, Cat# 289256-25G, 99.9%), thulium trichloride hexahydrate (Sigma-Aldrich, Cat# 204668-5G, 99.99%), ytterbium trichloride hexahydrate (Sigma-Aldrich, Cat# 337927-10G, 99.9%)], yttrium trichloride hexahydrate (Sigma-Aldrich, Cat# 464317, >99.99%), sodium hydroxide (Fisher Chemical, Cat# S318-500, Certified ACS, pellets), methanol (Fisher Chemical, Cat# A412-500, Certified ACS), ammonium fluoride (Sigma-Aldrich, Cat# 216011-100G, ACS Reagent, >98.0%), *n*-hexane (Macron Fine Chemicals, Cat# H487-10, 95%), nitric acid (Fisher Chemical, Cat# A200-500, Certified ACS Plus), toluene (Acros Organics, Cat# 32698-0010, >99.85%), ethanol (Ethyl alcohol, Sigma-Aldrich, Cat# 459844-1L, ACS Reagent, >99.5%, 200 proof), N,N-Dimethylformamide (DMF, Fisher Chemical, Cat# D119-500, Certified ACS), nitrosonium tetrafluoroborate ($NOBF_4$, Acros Organics, 97%, Cat# 174390050).

The Schlenk line (Cat# AF-0454) and other glassware was from ChemGlass. The temperature controller (Digi-Sense TC-9500) was from Cole-Parmer. The heating mantles (Cat# 100A-O963) were from Glas-Col. The vacuum pump (1400 DuoSeal) was from Welch. Si wafers were from Ted Pella (Ultra-flat, 6”, Cat# 21610-4, <100>, P/Boron-doped, 1-10 Ω/cm). TEM grids were from Ted Pella (Ted Pella, Cat# 01810, Carbon Type-B, 200 mesh).

Synthesis[1-4]:

Synthesis was performed in a 100 mL three-neck round-bottom flask (ChemGlass, heavy wall, Cat# CG-1524-A-10). Stirring was done using a magnetic egg-shaped stir bar (Spinbar, Cat# 371300034, teflon-coated, egg-shaped, ¾” x ⅜”). Initially, 4 mL of oleic acid (OA, Sigma-Aldrich, Cat# 364525-25ML, 90%, technical grade) and 6 mL of 1-octadecene (ODE, Sigma-Aldrich, Cat#

O806-1L, 90%, technical grade) were added to the round-bottom flask, followed by the addition of 0.4 mL total volume (0.4 mmol) of an aqueous solution of 1 M rare-earth (RE) chloride hydrates (see SI section “Materials” for catalog numbers) of desired ratios (first gray rectangle labeled “Add OA, ODE, RE salts” in Fig. S1). This solution was degassed three times with cycles of vacuum and argon purging in a standard Schlenk line setup (ChemGlass, Cat# AF-0454; vacuum pump: Welch, 1400 DuoSeal).

The temperature of the reaction was then set to 110 °C for 40 minutes using a temperature controller (Digi-Sense, TC-9500) with a thermocouple (Digi-Sense, Cat# EW-93600-22, Type-K) and a heating mantle (Glas-Col, Cat# 100A-O963) (blue rectangle labeled “Water removal, RE-oleate formation, ~100 °C” in Fig. S1). This step was needed to remove water from the reaction and prepare a precursor of oleate rare-earth salts. The heating mantle was then removed, and the solution was cooled to < 30 °C.

Next, a nucleation precursor solution was prepared by adding 1 mL of 1 M sodium hydroxide (Fisher Chemical, Cat# S318-500, Certified ACS, pellets; 1 mmol) in methanol (Fisher Chemical, Cat# A412-500, Certified ACS) to 4 mL of 0.4 M ammonium fluoride (Sigma-Aldrich, Cat# 216011-100G, ACS Reagent, >98.0%) in methanol (1.6 mmol) in a 50 mL centrifuge tube (Falcon, sterile, 50 mL polypropylene conical tube, 30 x 115 mm style, Cat# REF352070). Before mixing, each solution was dissolved in methanol and sonicated to homogeneity. The solutions were stored at 4 °C for future use. Note that in this protocol, the following ratios were used: fluorine to rare-earth ions ratio is 4:1; fluorine to sodium ratio is 4:2.5.

After mixing, the precursor solution was vortexed for 10 s and injected into the rare-earth oleate mixture through a septum (Sigma Aldrich, Cat# Z124621-100EA) using a syringe (Norm-Ject, 10 mL,Cat# REF 4100-000V0, Luer-lock) and a needle (Air-Tite Products Co., Inc., hypodermic needles, sterile, single-use, luer-lock, Cat# REF 8300014471) at room temperature under argon atmosphere (second gray rectangle labeled “Add NaOH, NH_4F, MeOH” in Fig. S1). The temperature was maintained at 50 °C under argon atmosphere for 40 minutes. After 40 minutes, the temperature was further increased to 80 °C and the reaction was either exposed to air or put under vacuum allowing methanol to evaporate. Once the temperature increased beyond the inflection point on the temperature *vs.* time plot of methanol evaporation, the reaction was slowly exposed to vacuum and the temperature was stabilized at 100 °C for 15 min under vacuum (these steps are shown in Fig. S1 as a cyan rectangle labeled “MeOH and resid. water removal, ~100 °C final T”).

After 15 minutes under vacuum, the reaction was placed under argon atmosphere and the temperature was increased to ~300 °C (or other desired temperature, usually in the 280-320 °C range). For $NaGdF_4$ nanoparticles, the growth temperature was 320 °C, while for $NaYF_4$ nanoparticles, the growth temperature was 300 °C. This heating step was achieved with a mean rate of ~15 °C/min (yellow rectangle in Fig. S1). The growth temperature was maintained for 60-90 minutes (60 min for $NaGdF_4$ and 90 min for $NaYF_4$ nanoparticles; red rectangle labeled “Nanoparticle nucleation (~10-20 °C/min) and growth at ~300 °C” in Fig. S1). After the reaction was complete, the heating mantle was removed, and the mixture was cooled down to < 30 °C. The entire volume of the reaction mixture was transferred to a 20 mL borosilicate glass scintillation vial (Fisher Scientific, Cat# FS74500) using a Pasteur pipette (Fisher brand, 9” disposable Pasteur pipettes, borosilicate glass, non-sterile, Cat# 13-678-20C). The samples were stored as-synthesized in 4 mL of oleic acid and 6 mL of 1-octadecene.

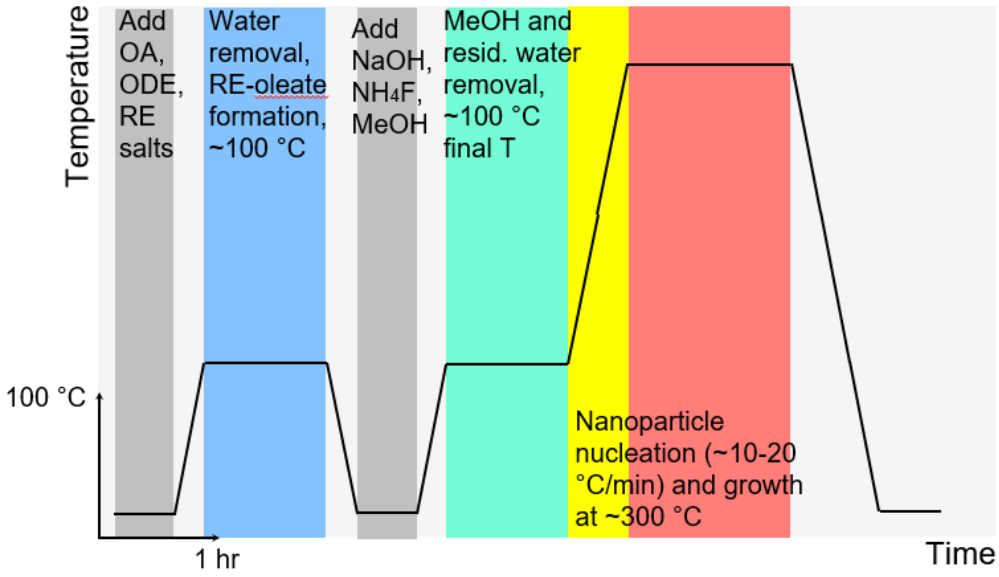

Figure S1. Schematic representation of major steps in rare-earth nanoparticle synthesis with time as an abscissa and temperature as the ordinate.

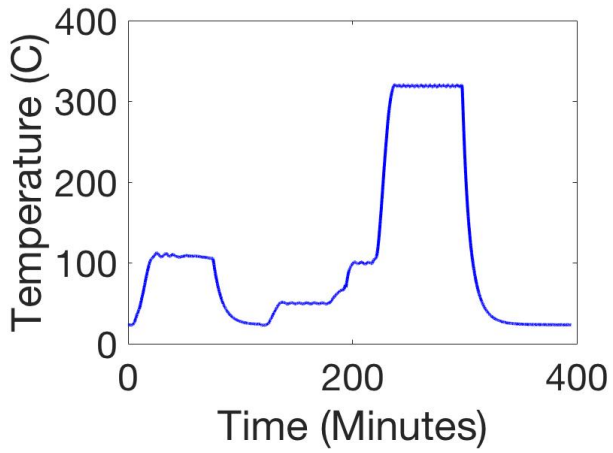

Figure S2. A typical temperature profile of a complete rare-earth nanoparticle synthesis reaction measured using the Digi-Sense TC-9500 temperature controller. The temperature sensor was placed in an NMR tube (Norell, Standard Series, Cat# C-505-P-7) that was inserted into the round-bottom flask through a rubber septum (Sigma Aldrich, Cat# Z124621-100EA).

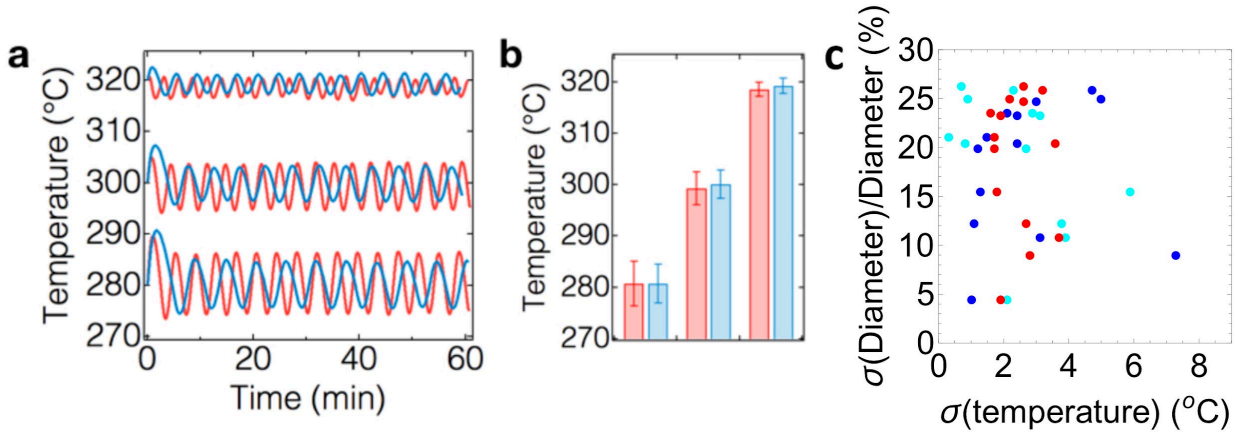

Figure S3. Temperature stability of the last high-temperature heating step in the rare-earth nanoparticle synthesis. (a) Typical temperature profiles for 280, 300, and 320 °C set temperature is shown. Blue and red colors represent temperature profiles obtained with two separate heating mantles and controllers. (b) The mean ± standard deviation were 280.7 ± 4.3, 299.4 ± 3.3, and 318.6 ± 1.3 °C for setup #1, and 280.8 ± 3.8, 300.2 ± 2.7, and 319.3 ± 1.4 °C for setup #2 for 280, 300, and 320 °C set points, respectively. (c) Variation in $NaGdF_4:Er^{3+}$ nanoparticle TEM diameter as a function of temperature stability. The color corresponds to the color code in Fig. S1, with blue indicating the water removal, cyan indicates MeOH/water removal, and red corresponds to nanoparticle growth.

Nanoparticle size and morphology characterization using TEM:

To wash a small portion of the reaction for TEM analysis, 0.5 mL of the as-synthesized nanoparticle solution stored in oleic acid and octadecene (4:6 by volume) was pipetted into a 1.5 mL Eppendorf centrifuge tube and 1:1 v/v 200 proof ethanol was added. The contents of the tube were mixed by shaking and inverting the tubes gently. The tubes were then centrifuged at 3 krcf (1 rcf = 1 g) for 3.5 min at 22 °C. The supernatant was discarded. The white pellets containing nanoparticles were resuspended in 300 µL 95% *n*-hexane each by vortexing. The resulting nanoparticle solutions were diluted by pipetting ~10-30 µL of the solution into an appropriate volume of 95% *n*-hexane to reach the total volume of 1 mL. The solution was then vortexed and 2 µL of it were applied to a copper/carbon/formvar TEM grid (Ted Pella, Cat# 01810, Carbon Type-B, 200 mesh). JEOL JEM1400 TEM at the Stanford Microscopy Facility was used for nanoparticle characterization. TEM images were analyzed using *ImageJ* to obtain the nanoparticle size. The image was imported into *ImageJ* and thresholded based on the intensity to identify the nanoparticles. The nanoparticles were identified using the "Analyze Particles" function. The nanoparticle area was then converted to TEM diameter assuming a perfectly spherical shape of the nanoparticles. The histogram of the nanoparticle TEM diameters was fit to a Gaussian function of the form $f(x) = Ae^{-\frac{(x-m)^2}{2\sigma^2}}$. The nanoparticle size is reported as the mean (m) of this Gaussian fit to the nanoparticle size histogram and the full-width-half-maximum (FWHM) of the nanoparticle TEM diameter distribution is $2\sigma\sqrt{2ln2} \approx 2.35\sigma$. TEM characterization of $NaGdF_4$ and $NaYF_4$ nanoparticles is shown in Fig. S4-S7.

Note that the method to extract the nanoparticle size described above was only used in TEM morphology analysis. Throughout the manuscript, the resulting value is referred to as the "TEM diameter". For CL imaging data, the nanoparticle size is referred to as the "nanoparticle SEM FWHM", which is equal to $2\sigma\sqrt{2ln2} \sim 2.35\sigma$, where σ is the standard deviation of a fitted 2-

dimensional Gaussian function (see section “Single-particle signal-to-noise ratio” below for details).

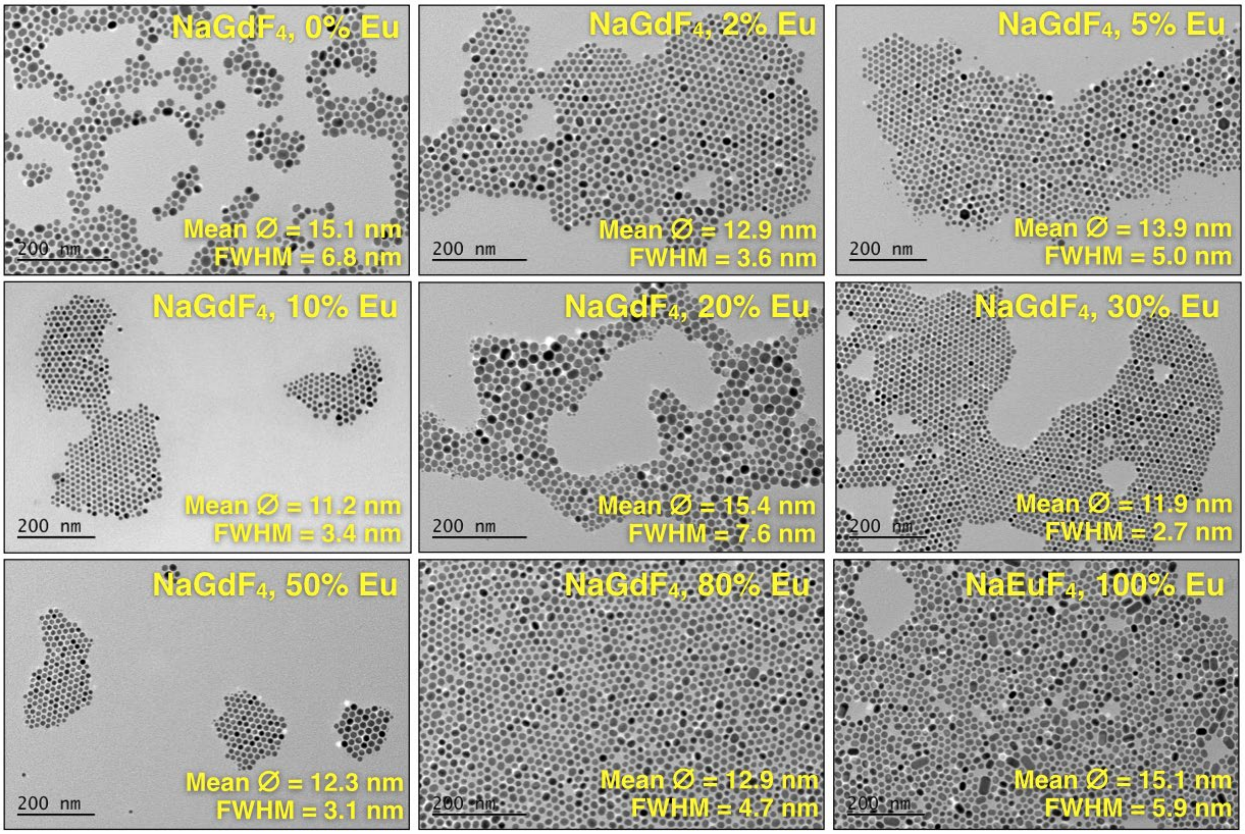

Figure S4. TEM characterization of a series of $NaGdF_4$ nanoparticles doped with Eu^{3+} at 0, 2, 5, 10, 20, 30, 50, 80, and 100 % doping levels. Mean TEM diameter and the FWHM of the nanoparticle TEM diameter distribution are shown for each sample.

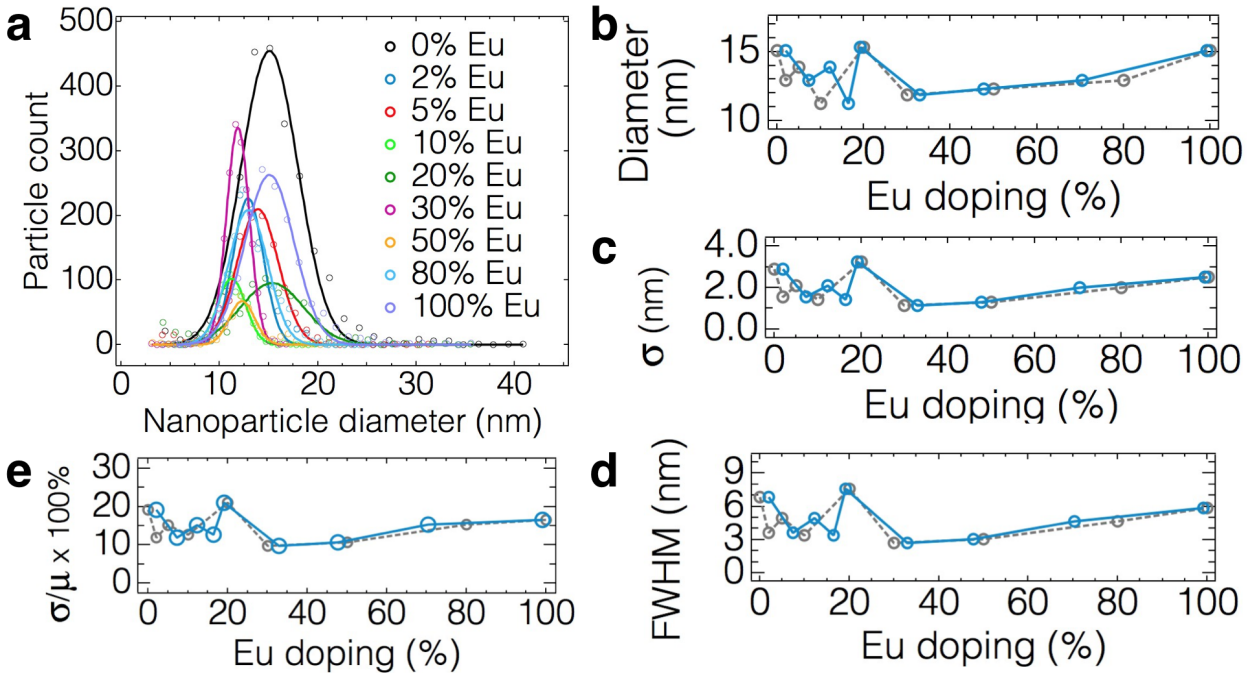

Figure S5. Nanoparticle size characterization for a series of $NaGdF_4$ nanoparticles doped with Eu^{3+} and different doping levels. (a) Histograms of nanoparticle TEM diameter (circles) fit to a Gaussian distribution (solid lines). TEM diameter (b), standard error (c), FWHM of the nanoparticle TEM diameter distribution (d), where FWHM of the nanoparticle TEM diameter distribution = $2\sigma\sqrt{2ln2}$, and the percent ratio of the standard error and the TEM diameter (e), which is sometimes referred to as the polydispersity index.

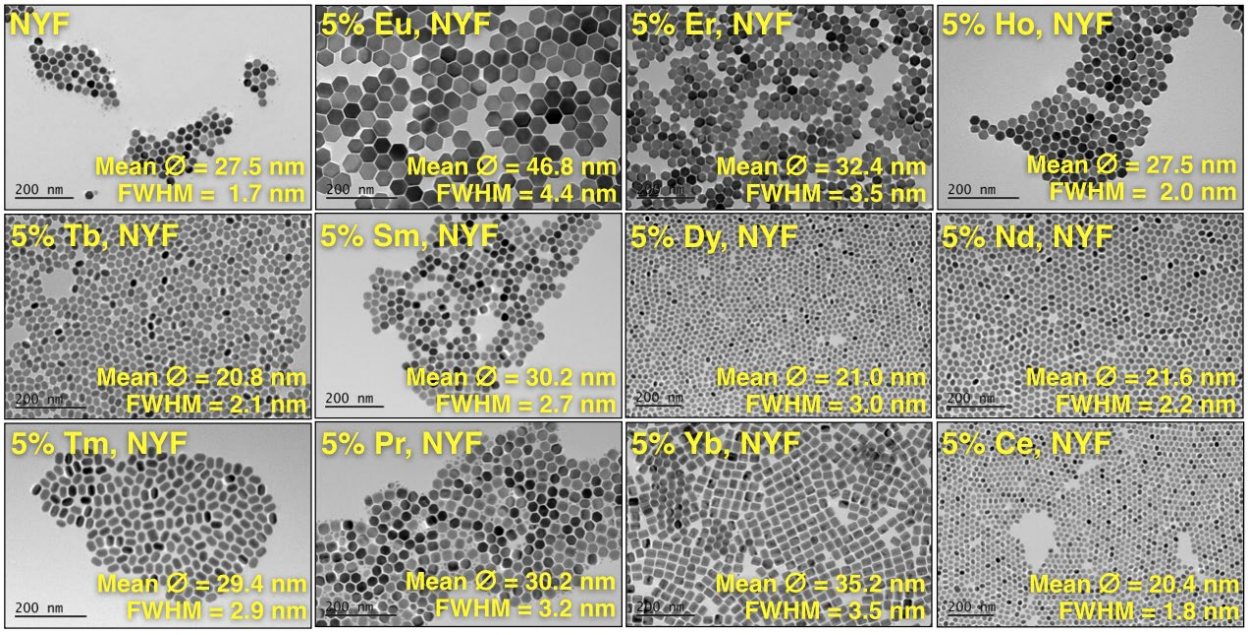

Figure S6. TEM characterization of a series of $NaYF_4$ nanoparticles doped with different rare-earth ions. Mean TEM diameter and the FWHM of the nanoparticle TEM diameter distribution are shown for each sample.

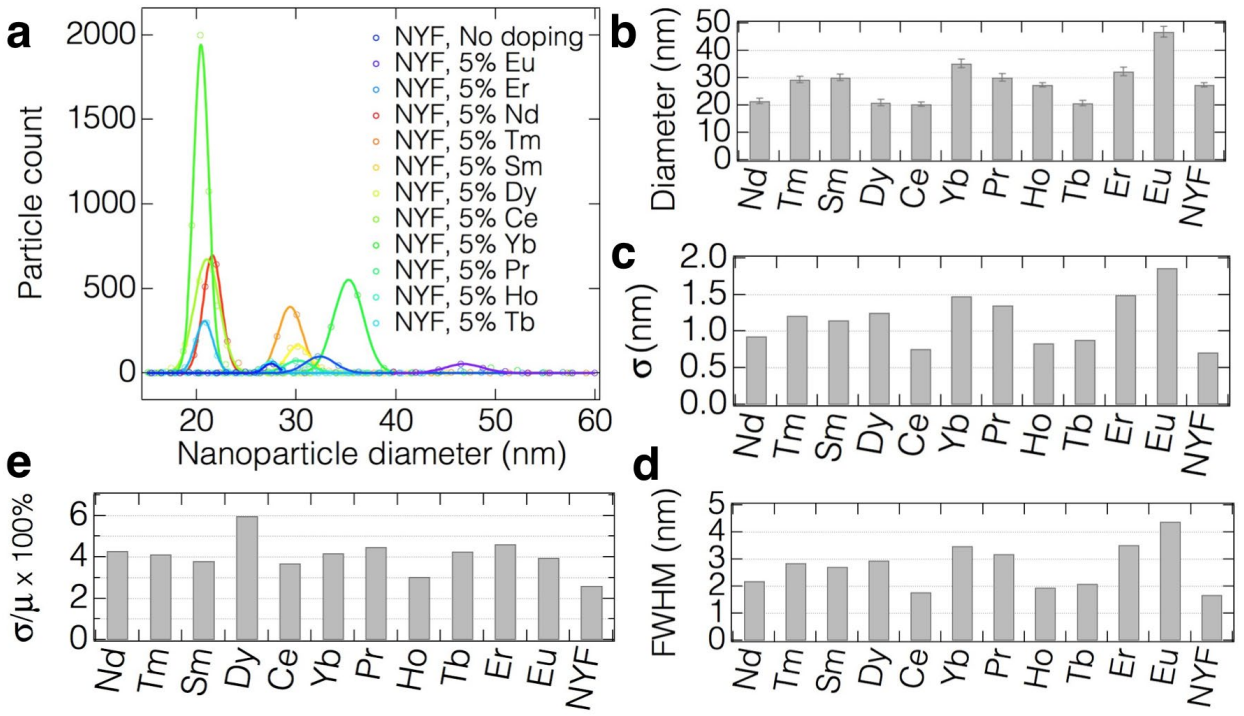

Figure S7. Nanoparticle size characterization for a series of $NaYF_4$ nanoparticles doped with various dopants at 5% level. (a) Histograms of nanoparticle TEM diameter (circles) fit to a Gaussian distribution (solid lines). TEM diameter (b), standard error (c), FWHM of the nanoparticle TEM diameter distribution (d), where FWHM of the nanoparticle TEM diameter distribution = $2\sigma\sqrt{2ln2}$, and the percent ratio of the standard error and the TEM diameter (e), which is sometimes referred to as the polydispersity index.

Nanoparticle characterization by inductively-coupled plasma mass spectrometry (ICP-MS):

The nanoparticles were first washed by adding 0.5 mL of as-synthesized nanoparticles in oleic acid and octadecene solution to 0.5 mL of ethanol in a 1.5 mL Eppendorf tube and centrifuging at 3.5 g for 3 min at room temperature. This wash was repeated two more times to ensure that no residual rare-earth salts remain in the solution. After each wash, the nanoparticles were dissolved in 0.5 mL 95% *n*-hexane. After the last wash, the supernatant was discarded and 50 µL of ethanol were added to the pellet. The pellet was resuspended as much as possible using vigorous vortexing and sonication. 2 mL 100% ACS reagent 35% HNO_3 was added to the ethanol suspension of nanoparticles. Mixing of nanoparticles in ethanol with HNO_3 is highly exothermic. It is important that the acid is added slowly and carefully to the nanoparticle solution, wear proper PPE (face shield) and work in the fume hood. The solution was sonicated for 1 hour and was incubated at room temperature for 24 hours. The solution was then diluted by ~50x and 2 µL of the solution were applied to a TEM grid (Ted Pella, 01810, Carbon Type-B, 200 mesh) to check if the nanoparticles were dissolved. 20x, 2000x, and 200,000x dilutions of the sample in 1.75% HNO_3 were prepared for ICP-MS analysis. A blank solution of 1.75% HNO_3 in H_2O was prepared by pipetting 5 mL of 70% HNO_3 into 195 mL of H_2O. Four standard solutions with 10 ppb, 100 ppb, 1 ppm, and 10 ppm ion concentration in 1.75% HNO_3 were also prepared. All solutions were filtered with 0.22 µm syringe filter before ICP-MS analysis. Thermo Scientific XSERIES 2 Quadrupole ICP-MS in the Stanford Environmental Measurements Facility was used for ICP-MS analysis. Note that BF_4-exchanged nanoparticles can also be used for ICP. This approach may

be even better because BF_4-exchanged nanoparticles are soluble in polar solvents and DMF is miscible with HNO_3.

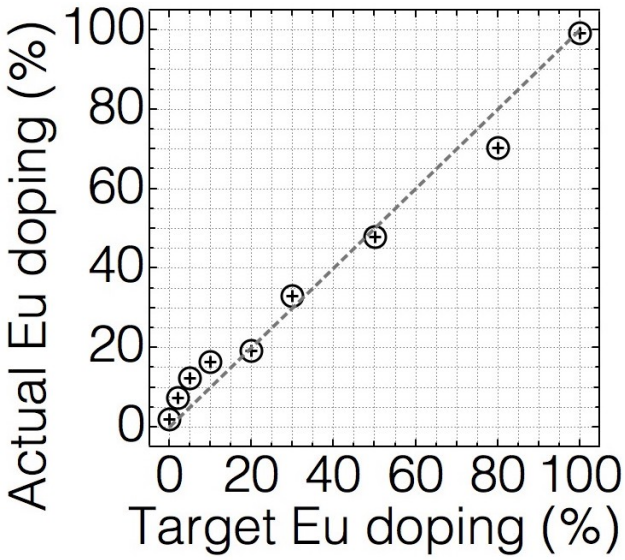

Figure S8. Inductively-coupled plasma-mass spectrometry analysis of $NaGdF_4$ nanoparticle doping levels of Eu^{3+}.

Cathodoluminescence electron microscopy measurements

Ensemble measurements of nanoparticle properties may be compromised by artifacts such as aggregation which could affect the luminescent properties, or may suffer from systematic errors such as an uncertainty in nanoparticle concentration. Therefore, we sought to perform single-particle cathodoluminescence measurements on the rare-earth nanoprobes to evaluate them for the ultimate use in single-particle multicolor electron microscopy.

CL instrument:

Single-nanoparticle CL measurements were done at the Molecular Foundry at the Lawrence Berkeley National Laboratory. Experiments were performed on a Zeiss Supra 55-VP-FESEM with a cathodoluminescence parabolic mirror light collection system constructed by the Imaging and Manipulation Facility of the Molecular Foundry at the Lawrence Berkeley National Laboratory. A 1.3π sr (1 mm focal length) diamond-turned aluminum parabolic reflector mounted on a 4-axis high vacuum nanopositioning stage (Attocube, ECSx3030 for *X*, *Y*, and *Z* translation; Attocube, EGCt5050 and EGCp5050 for pitch and yaw, respectively) was used to collimate the light emitted from the sample and direct it through a window consisting of a fused silica optical flat mounted in the side of the SEM vacuum chamber. The light was then focused onto an IR enhanced, Peltier cooled photomultiplier counting module (Hamamatsu H7442-40) with a 50 mm focal length achromatic doublet. For the description of the scanning software, see ref. [5]. Access to the instrument was provided through Molecular Foundry proposals #3349, #3942, #4387 and #5208.

Single-particle CL sample preparation:

For the single-nanoparticle CL measurements, the nanoparticles were exchanged into dimethylformamide (DMF, Fisher Chemical, Cat# D119-500, Certified ACS) using a modification of a published procedure[6]. In a 1.5 mL Eppendorf centrifugation tube (Eppendorf, safe-lock tubes, 1.5 mL, Cat# 022363204), 0.5-1 mL of as-synthesized nanoparticles were mixed with an equal

volume of ethanol (Sigma-Aldrich, Cat# 459844-1L, ACS Reagent, >99.5%, 200 proof) and washed by centrifugation at 3,500 g for 3 minutes. The pellet was resuspended with 0.5 mL *n*-hexane (Macron Fine Chemicals, Cat# H487-10, 95%) and the 0.5 mL ethanol wash was repeated. The pellet was then resuspended in 0.3 mL of *n*-hexane and 0.3 mL of nitrosonium tetrafluoroborate ($NOBF_4$, Acros Organics, 97%, Cat# 174390050) in DMF was added. The phase-separated liquid was inverted continuously for 45 minutes using a laboratory shaker. No trend in single-nanoparticle CL brightness as a function of $NOBF_4$ incubation time was observed (Fig. S9a). After 45 minutes, the tube was centrifuged at 10,000 g for 10 minutes and the supernatant was discarded. The pellet was washed with 0.2 mL of a 1:1 mixture of toluene (Acros Organics, Cat# 32698-0010, >99.85%) and *n*-hexane by vortexing and centrifugation at 10,000 g for 10 minutes. The resulting pellet was dried under argon and the nanoparticles were resuspended in 0.1-0.2 mL of DMF. No trend in single-nanoparticle CL brightness as a function of DMF incubation time was observed (Fig. S9b). 4 µL of nanoparticles in DMF were pipetted in the center of a ~5 x 5 mm piece of a silicon wafer (Ted Pella, ultra-flat, 6", Cat# 21610-4, <100>, P/Boron-doped, 1-10 Ω/cm) and spin-coated within 15 seconds of droplet deposition. Spin-coating was done with a G3 instrument (Speedline Technologies) for 1 min using 5 s acceleration time, 5 s deceleration time, and 3000 rpm spinning speed. The sample was checked under SEM and adjustments to the concentration were made to achieve a density compatible with imaging several single nanoparticles within a 1 μm^2 region. When the desired concentration was found, a fresh sample of an identical concentration was prepared for the single-nanoparticle CL measurements.

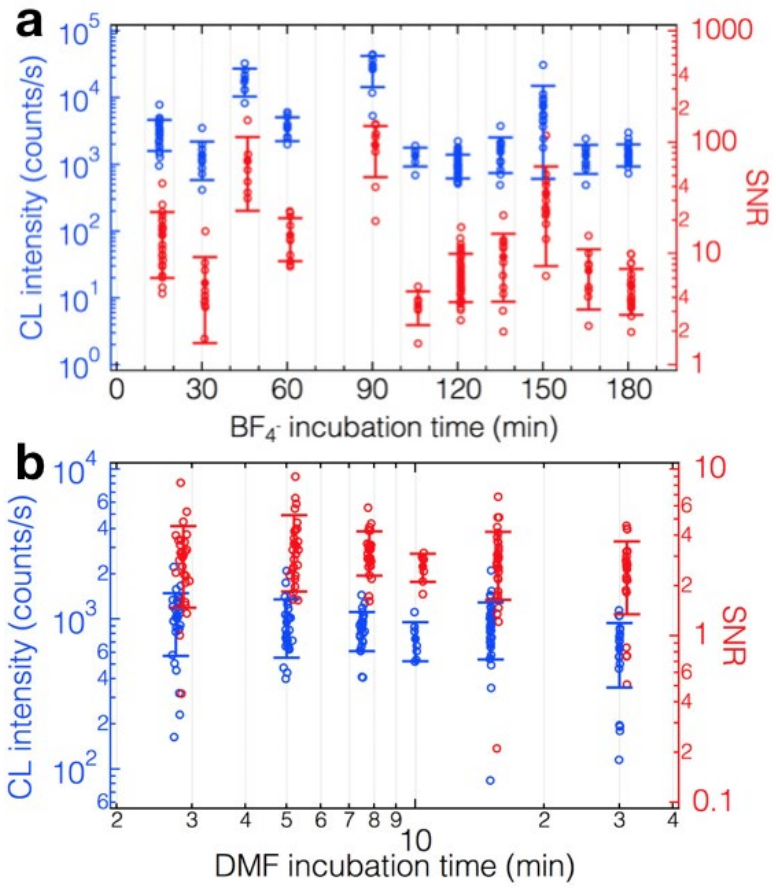

Figure S9. Single-particle CL measurements of $NaGdF_4$:5%Eu^{3+} nanoparticles as a function of incubation time in BF_4^- (a) and DMF (b). Each blue empty circle corresponds to a single nanoparticle within a 1 μm^2 field of view and represents the brightness (Gaussian amplitude) in counts per second (blue, y-axis on the left). Each red empty circle represents the signal-to-noise ratio for each nanoparticle (red, y-axis on the right). Filled circles represent the average brightness in counts per second (blue, y-axis on the left) and the CL signal-to-noise ratio (CL SNR, red, y-axis on the right). Error bars represent one standard deviation from the mean.

Background CL noise is described by Poisson statistics:

The properties of the background CL signal were analyzed by repetitively scanning the same sample region (N = 25). For this study, the sample consisted of $NaGdF_4$:Eu^{3+} nanoparticles spin coated on a paraformaldehyde- and glutaraldehyde-fixed OsO_4-stained HeLa cell. The scanned region was 178 nm away from the nearest nanoparticle, and most of the background luminescence could be attributed to auto-luminescence from the sample substrate. Fig. S10 shows the average detected CL signal as a function of number of accumulated frames (N). Each frame consists of a region of 32 x 32 pixels and a pixel integration time of 500 µs. The accumulated signal (Fig. S10a) scales linearly with the number of frames and can be approximated by a linear fit ($150\frac{\text{photons}}{\text{frame}}N$). In Fig. S10b, the standard deviation of the signal increases sub-linearly as a function of accumulated frames and is accurately represented by a model described by shot-noise (black line $\sqrt{150\frac{\text{photons}}{\text{frame}}N}$). In the set of data given in Fig. S10, the average accumulated counts in a region of 32 x 32 pixels was ~1.5 x 10^5, with the fractional shot noise ~ $\frac{1}{\sqrt{N}}$= 0.0026. For the data shown in the Main Text in Fig. 2 and Fig. 3, the number of pixels used to establish the background was typically of the same order.

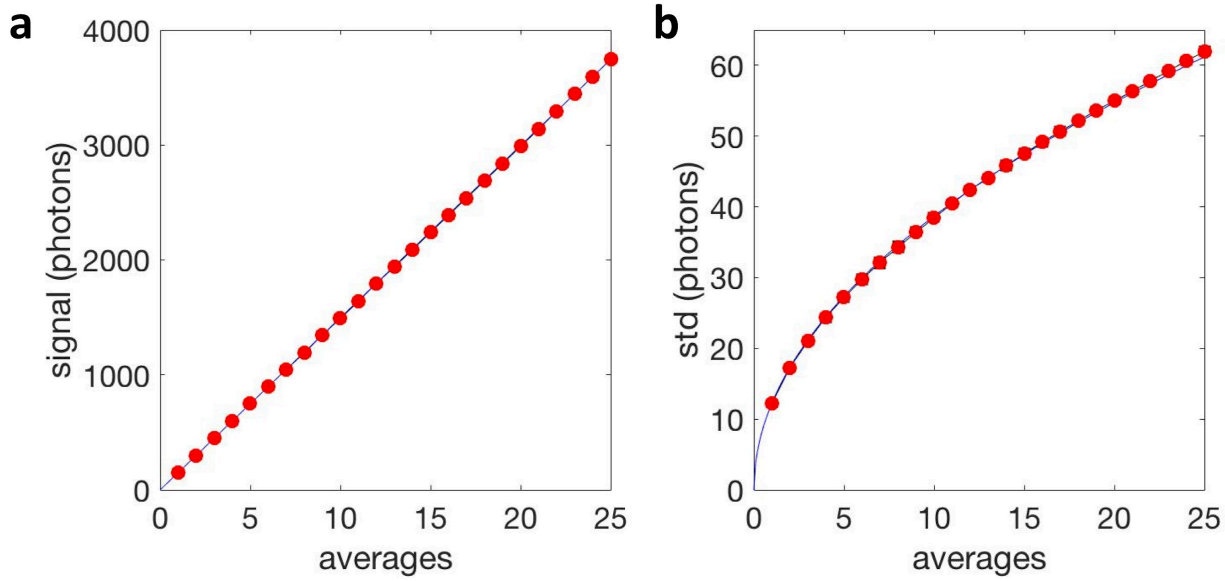

Figure S10. (a) Per pixel CL-signal (red points) for an accumulation of N frames containing 32 x 32 pixels, and corresponding linear fit (black line). (b) standard deviation (red points) of a frame and expected noise based on the signal in (a) (black line).

CL noise scaling of individual nanoparticles:

A similar analysis is repeated for the CL signal of individual $NaGdF_4$ nanoparticles doped with 5% Eu. The particles were dispersed on a Si wafer and imaged at 5 kV acceleration voltage and 2 ms pixel integration time. Figure SXX shows the scaling of the CL signal (a) and noise (b) of nanoparticles as a function of integration time. In (a), The CL signal was calculated by fitting a Gaussian function with $G(x_i, y_i) = c_o + c_1 y_i + c_2 x_i + Ae^{\frac{-(x_i - x_o)^2 - (y_i - y_o)^2}{2\sigma^2}}$ (see Main Text methods section "Single-nanoparticle cathodoluminescence data analysis" for definition of the fit parameters), and integrating the CL signal for all pixels within a 2σ distance from the center of the nanoparticle. The standard deviation in (b) was calculated as $\left(\Sigma_{(x_i-x_0)^2+(y_i-y_0)^2<4\sigma^2}\left(I(x_i, y_i) - G(x_i, y_i)\right)^2\right)^{1/2}$, where $I(x_i, y_i)$ represents the number of detected photons in pixel at location (x_i, y_i) and (x_0, y_0) the particle location. Figure SXXb indicates that the standard deviation exceeds the expected $\sqrt{G(x_i, y_i)}$ based on Poisson distribution by $(58 \pm 8)\%$. Note that this decrepancy can either originate from fluctuations in the particles CL emmision rate or from discrepancies of the fit $G(x_i, y_i)$ from the true point spread function.

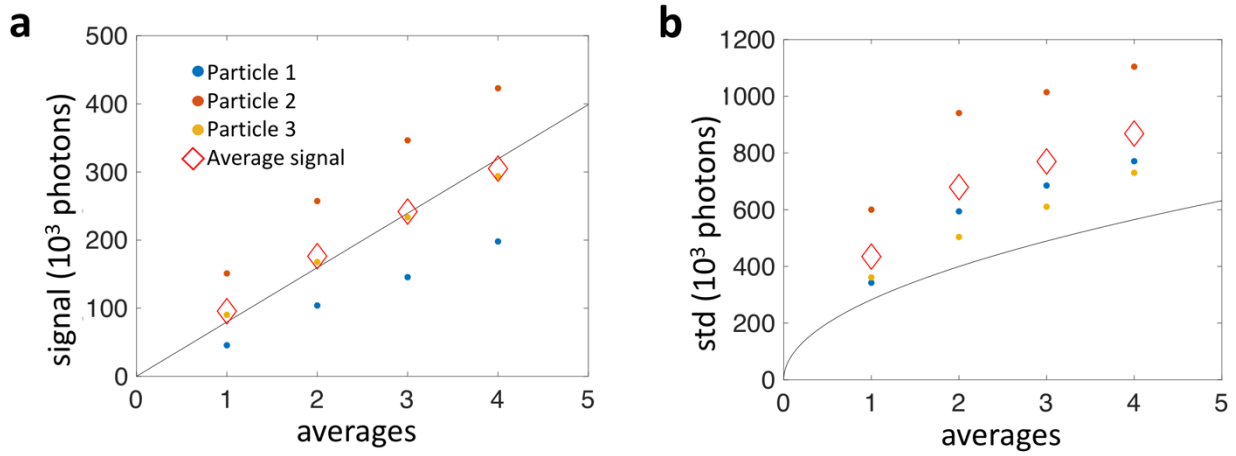

Figure S11. (a) CL-signal of individual nanoparticles (blue, red, and orange points) and average of CL-signal for all three particles (red diamonds), for an accumulation of up to 4 frames. The black line corresponds to a linear fit. (b) Standard deviation, as defined in the text, for individual nanoparticles (blue, red, and orange points) and their average (red diamonds). The black line indicates the expected noise based on Poisson noise for the signal in (a).

Single-particle signal-to-noise ratio:

In order to extract the CL intensity and signal-to-noise ratio for individual particles, a sub-region within the original 1 μm² field of view containing one or several individual particles was selected. Nanoparticle aggregates were deliberately avoided in this analysis. For the case when a single nanoparticle was selected in the SEM image, its raw CL image was $I(x_i, y_i)$, where x_i and y_i are discrete pixels of 1.95 nm pitch and the total size of each image is 512 x 512 pixels. Thus, $I(x_i, y_i)$ represents the counts per pixel recorded during the time when the electron beam was irradiating each pixel. Then, $I(x_i, y_i)$ was fitted to a two-dimensional Gaussian function with a linearly sloped background of the form $G(x_i, y_i) = c_o + c_1 y_i + c_2 x_i + Ae^{\frac{-(x_i - x_o)^2 - (y_i - y_o)^2}{2\sigma^2}}$ (Fig. S12). In the case when multiple nanoparticles are present in the selected sub-region, extra Gaussian functions

are added to a global fit of several nanoparticles that share the same background. The standard deviation and the center x_o and y_o positions of the Gaussian fit were obtained by fitting the SE2 signal of the same nanoparticle and using these values as the starting point in the fit of the CL image. The standard deviation of the CL image of the nanoparticle was constrained to not deviate by more than 10 % from the SE2 image of the same nanoparticle. The Gaussian component of the fitted function $S(x_i, y_i) = Ae^{\frac{-(x_i-x_o)^2-(y_i-y_o)^2}{2\sigma^2}}$ represents the CL signal of an individual nanoparticle. The sum of $S(x_i, y_i)$ gives the number corresponding to the number of counts associated with each particle. However, since the "counts" are derived from a fitted function, the integral need not be an integer. The signal-to-noise ratio was calculated by first summing up the CL signal of the nanoparticle $S_{total} = \sum_i S(x_i, y_i)$ including only the pixels in which the signal is greater than a defined threshold, which is commonly taken as the signal at pixels 2σ (95% confidence level) away from the center of the Gaussian distribution. The threshold of 2σ was used because it is ideal when the background level is equal to the amplitude of the Gaussian of the fitted CL signal, which is the case for the data collected in this work. The noise was calculated for the same pixels as $N_i = \sqrt{G(x_i, y_i)}$ and the total noise was determined by adding the noise for each pixel in quadrature: $N_{total} = \sqrt{\sum_i N_i^2}$. The overall signal-to-noise ratio for a single nanoparticle was then defined as the ratio $SNR = \frac{S_{total}}{N_{total}}$. We note that other approaches to determining the SNR and smoothing the imaging data using optimal filtering functions instead of a simple top-hat function exist, but the approach described above was chosen because it is consistent with the previous literature on single-molecule localization microscopy.

The SEM nanoparticle full-width-half-maximum (FWHM) was calculated from the standard deviation, σ, as SEM FWHM = $2\sigma\sqrt{2\ln 2} = 2.35\sigma$. Note that, strictly speaking, this analysis is fully accurate only when the signal can be perfectly described by a Gaussian function. However, deviations from this behavior can occur due to a non-spherical shape of the nanoparticle or due to astigmatism and sample drift. Astigmatism and sample drift result from sample charging when organic material is present on the sample surface and imaging is done at low beam energy.

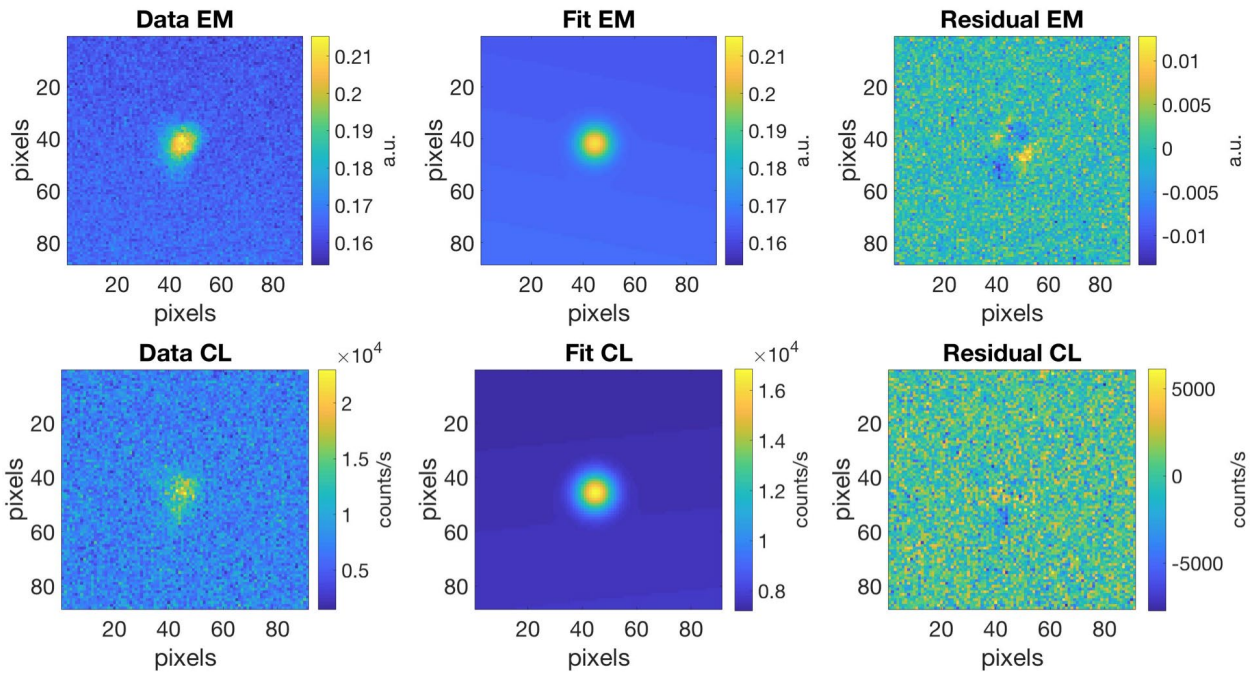

Fig S12. Example of a 2D Gaussian fit for the CL of a single $NaGdF_4$:5% Eu^{3+} nanoparticle. Top row shows the raw data (left), 2D Gaussian fit (center), and the residual (right) for the SE2 secondary electron signal. The bottom row shows the corresponding images for the CL signal of the same nanoparticle. Pixel pitch is 1.95 nm; pixel dwell time is 2 ms; beam energy is 5 keV; beam current is ~400 pA.

In order to validate the described Gaussian fitting algorithm and explore its limitations in the context of identifying a nanoparticle in a specific color channel, we have conducted simulations of the signal and used the same fitting procedure that we used for the CL data to fit the simulated data (Fig. S13). For each simulation, one hundred 31 x 31 pixel images were generated that either contained only the background of various intensity (Fig. S13a-b) or both the background and the Gaussian signal with an amplitude equal to the amplitude of the background, the standard deviation of 4 pixels (similar to the data for $NaGdF_4$:Eu^{3+} nanoparticles), and the center of the Gaussian peak at the very center of the simulated image (Fig. S13c-d). The simulated images contained Poisson shot noise. In both cases, the simulated images were fitted with a single Gaussian function with a standard deviation of 4 pixels, which is comparable to the data for $NaGdF_4$ nanoparticles. The fit was performed such that both positive and negative values of the Gaussian amplitude were allowed (red data) and so that only the positive values were allowed (blue data). The latter procedure was used to fit all the CL data in this work.

These simulations suggest that noise can result in erroneous identification of CL signal (Fig. S13a). However, the magnitude of this signal is small, such that the resulting fit would only have the signal-to-noise ratio of up to ~2 (95% confidence, Fig. S13b). In the case when the amplitude of the signal is equal to the amplitude of the background (Fig. S13c-d), the fitting procedure only overestimates the signal at very low signal levels (up to the Gaussian amplitude of <1 count, which is equivalent to <500 counts/s for a 2 ms pixel dwell time used in most of our CL imaging experiments). Therefore, since the positive identification of a nanoparticle can be done using SE2 or back-scattered electron signal and the Gaussian fitting only becomes unreliable at CL SNR < 2, the CL SNR values between 2 and 5 (the latter given by the Rose criterion) can also be used for the identification of the nanoparticle color in addition to the larger CL SNR values.

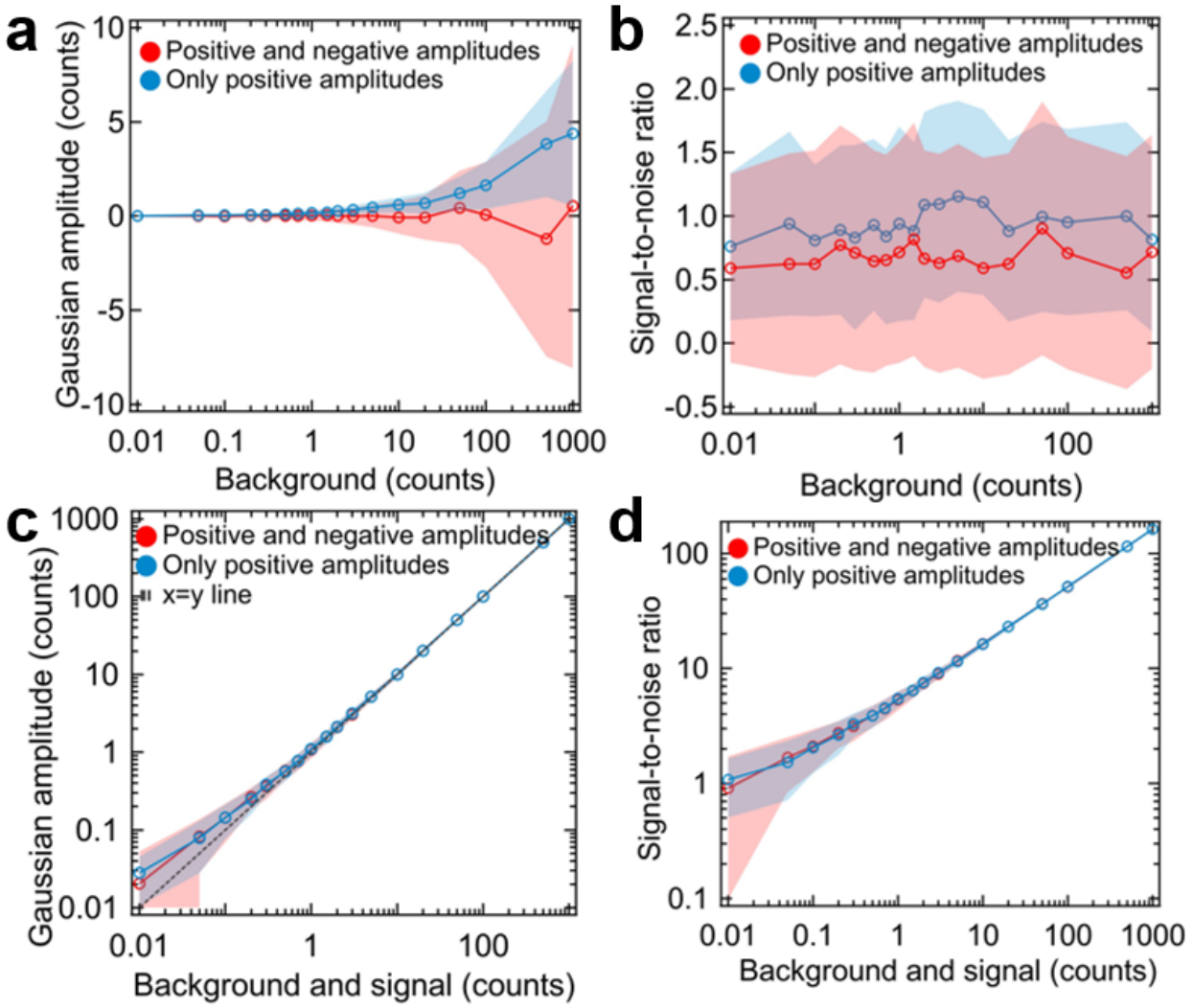

Figure S13. Gaussian fitting of simulated CL data. In each case, one hundred 31 by 31 pixel images were generated and fitted. The data show the mean and the one standard deviation spread around the mean. In panels (a-b), the simulated images contained only the background with an average number of counts shown on the x-axis and distributed according to the Poisson statistics. No Gaussian signal was present in these images. The images were fit with a single 2D Gaussian function with an amplitude that could take on both positive and negative values (red data) or positive values only (blue data). Gaussian amplitudes of the fits are shown in panel (a) and the signal-to-noise ratio is shown in panel (b). In panels (c-d), in addition to the background, the simulated images contained a Gaussian signal with a standard deviation of 4 pixels and equal in amplitude to the background.

Measurements and analysis of the electron beam sample interaction volume:

In electron microscopy, the electron interaction volume inside a substrate is strongly voltage-dependent. Therefore, the extent to which the imaging resolution is affected by stray electrons scattered in the substrate was explored. This was accomplished by imaging a large ~180 nm SEM FWHM Eu^{3+}-doped vanadate oxide (YVO_4:10% Eu^{3+}) nanoparticle at beam energies ranging from 1.5 to 20 keV (Fig. S14). Cross-sectional line profiles of the CL signal of this nanoparticle are shown in Fig. S14b. In addition to the CL signal resulting from direct primary beam excitation, a

voltage dependent “halo” appears in the regions proximal to the nanoparticle. A double-Gaussian model was used to fit the line profiles in Fig. S14b and the widths of the two Gaussians were plotted in Fig. S14c (blue and red). The Gaussian width representing primary beam excitation of the nanoparticle is shown in blue; the Gaussian width representing the stray excitation halo is shown in red. While the primary beam excitation Gaussian has a similar width across all voltages (blue), the “halo” Gaussian width increases with voltage (red) (see Fig. S15 for Gaussian intensities of the signal and the “halo”). In addition, the background intensity increased by approximately 2 kcps/keV in this measurement (Fig. S14c, green).

These results suggest that imaging lanthanide nanoparticles at low electron landing energy minimizes the background by reducing the CL “halo” that originates from stray electron excitation by electrons backscattered from the silicon substrate. The observed halo is more pronounced at the intermediate voltages of 5-15 keV and not at 20 keV (Fig. S14b). The data in Figure S13b shows how the background counts increase 20-fold as the energy is varied between 1.5 kV to 20 kV. The FWHM of the “halo” also broadens as the electron interaction volume within the substrate begins to span many microns.

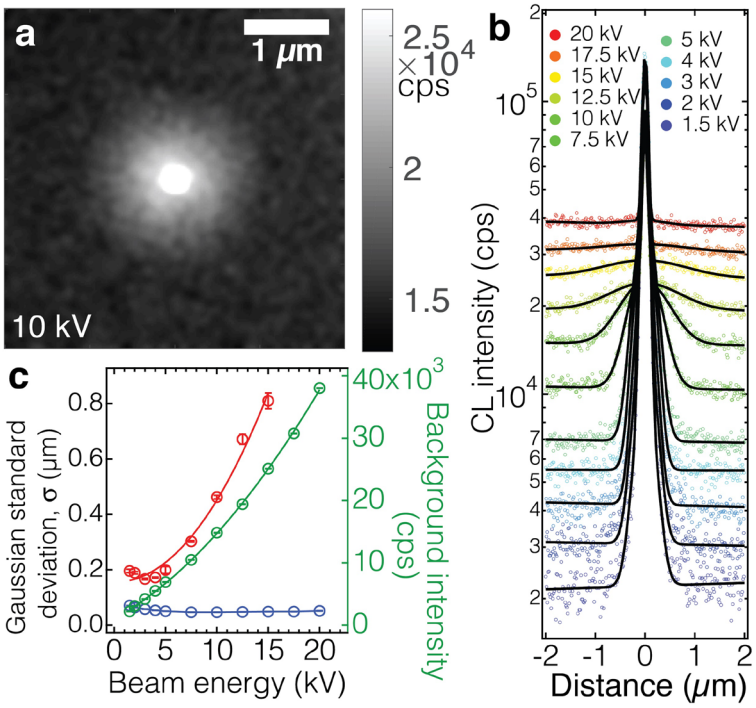

Figure S14. Optimization of imaging conditions in cathodoluminescence microscopy. (a) A CL image of a single YVO_4:10% Eu^{3+} nanoparticle of ~180 nm SEM FWHM acquired using 10 keV beam energy. The color scale is adjusted so that the nanoparticle itself is saturated (white spot in the center) and the background “halo” around the nanoparticle is visible. The image is 4 × 4 μm; the pixel pitch is 15.8 nm; dwell time per pixel is 2 ms; a Gaussian smoothing filter with one standard deviation of 47.4 nm (three pixels) was applied. (b) Cross-sectional line profiles of the same nanoparticle imaged at various beam energies (including 10 keV). The width of a CL “halo” around the nanoparticle increases with beam energy (data in rainbow colors). Double-Gaussian fits of the data are shown as black lines. (c) Double-Gaussian fits of the nanoparticle imaged at different beam energies. Gaussian standard deviation (blue and red, left axis), and background intensity (green, right axis) of the same measurements shown as line profiles in panel (b). Data in blue represents the standard deviation of the “signal” Gaussian; data in red represents the

standard deviation of the "halo" Gaussian. "Halo" Gaussian amplitude data are fit to a power law: $(0.155 \pm 0.022) + (0.0025 \pm 0.0019)(\text{keV})^{2.06 \pm 0.27}$. Background intensity data are fit to a polynomial $(1042 \pm 187) + (900 \pm 48)x + (47 \pm 2)x^2$ as a guide for the eye.

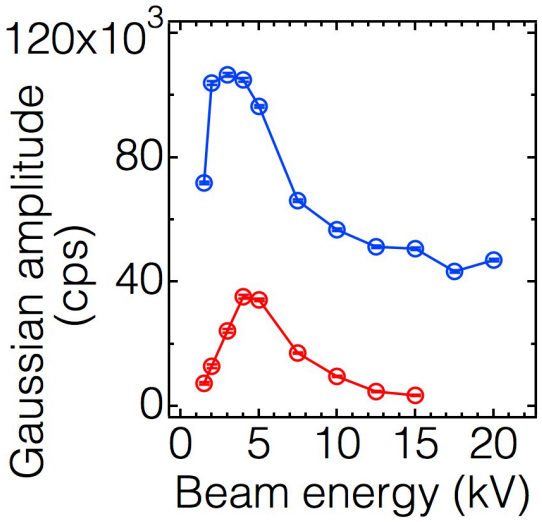

Figure S15. Double-Gaussian fit amplitudes of a single 180 nm SEM FWHM 10% Eu^{3+}:YVO_4 nanoparticle imaged at different beam energies. The figure shows Gaussian intensity amplitudes for the "signal" (blue) and the "halo" (red) as a function of the electron beam energy.

Electron energy loss in a material can be described by the Bethe formula: $\frac{dE}{ds} = -7.85 \times 10^4 \frac{Z\rho}{AE_i} \ln\left(\frac{1.166E_i}{J}\right)$, where $\frac{dE}{ds}$ is in the energy loss of an electron per traveled distance in $\frac{keV}{cm}$, Z is the atomic number, ρ is the density in $\frac{g}{cm^3}$, A is the atomic weight in $\frac{g}{mole}$, E_i is the electron energy in keV, and J is the average loss in energy per event[7] in keV that depends on the atomic number such that $J = (9.76\,Z + 58.5\,Z^{-0.19}) \times 10^{-3}$.

This equation has been modified by Joy and Luo[8] for energies <5 keV to replace J by J^* such that $J^* = \frac{J}{1 + (kJ/E_i)}$, where J is the value given by the conventional expression and k is a variable dependent on the atomic number: $k = 0.731 + 0.0688 \log_{10} Z$.

In addition, the Kanaya-Okayama formula[9] has been widely used to calculate the range of the electron interaction volume: $R_{KO}(\mu m) = \frac{0.0276A}{Z^{0.89}\rho} E_o^{1.67}$.

We have calculated electron energy loss using both the Bethe formula and the Kanaya-Okayama formula (Fig. S16b).

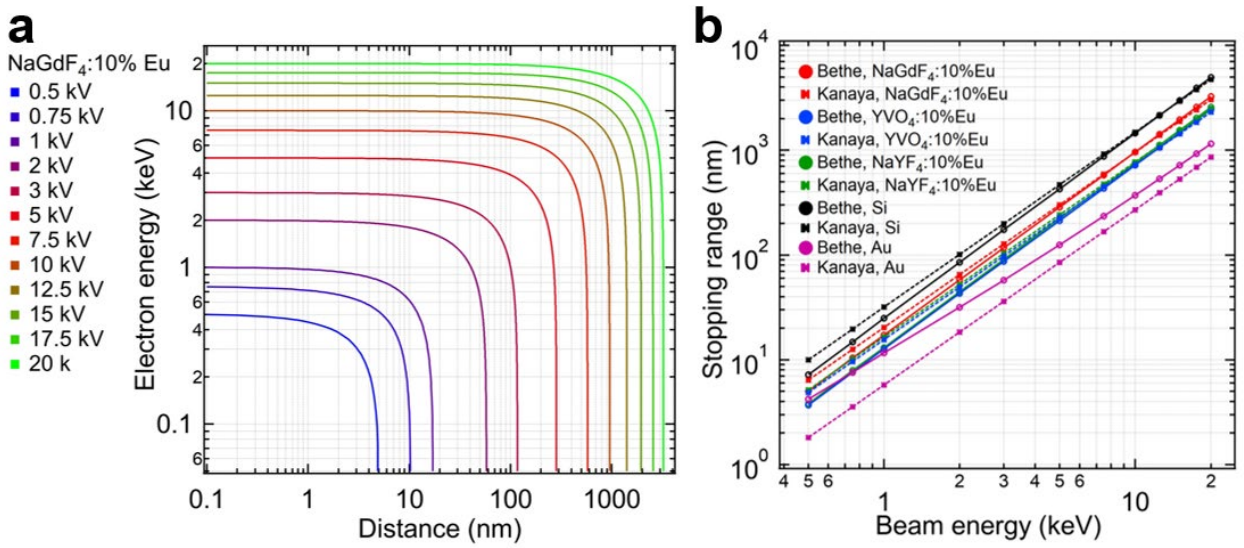

Figure S16. Electron interaction range in rare-earth-doped materials as predicted by the Bethe formula and the Kanaya-Okayama formula. (a) Electrons of various initial energies (legend on the left) dissipate energy as they pass through $NaGdF_4$:10% Eu^{3+}. The Bethe stopping range is defined here as the travel distance in the material at which the electron energy becomes equal to zero. (b) Stopping range at various energies as predicted by the Bethe formula (solid lines, open circles), and the Kanaya-Okayama formula (dashed lines, stars) for gold (magenta), silicon (black), $NaYF_4$:10% Eu^{3+} (green), YVO_4:10% Eu^{3+} (blue), and $NaGdF_4$:10% Eu^{3+} (red). Note that the atomic numbers and the atomic weights were calculated as an average of all atoms in rare-earth-doped materials.

Incident electron energy to optimize the CL SNR

From Fig. S16, at an incident energy of 1 keV, the stopping distance is ~16 nm, comparable to the diameter of our $NaGdF_4$ nanoparticles. Good SEM contrast is achievable at an operating energies as low as 1.0-1.2 keV. Fig. S14 indicates that the background counts will continue to decline at energies below 1.5 keV. These data indicate that the combined maximum SEM image quality and CL SNR will be achieved in the range of energies ~1.0 -1.2 keV.

Single-particle CL measurements:

A routine single-nanoparticle CL measurement included the alignment of the CL mirror in the *X*, *Y*, pitch, and yaw axes, as well as optimizing the height of the sample relative to the CL mirror. The alignment was done using a sample of YVO_4:10% Eu^{3+} nanoparticles of broad size distribution in the 40-250 nm range on a piece of silicon wafer. The brightest particles in this sample allowed collecting ~7 x 10^5 counts/second using standard operating conditions. The working distance was in the 4.9-5.2 mm range, the current was on the order of 300-500 pA, and the beam energy was 5 keV. The samples were scanned using a 512 x 512 point grid of 1 μm x 1 μm dimensions resulting in a pixel pitch of 1.95 nm. The dwell time per pixel was either 500 μs or 2 ms depending on the experiment and expected count rates. The estimated electron dose under these conditions was approximately 5,000-20,000 electrons/$Å^2$ (current density ~100 pA/nm^2).

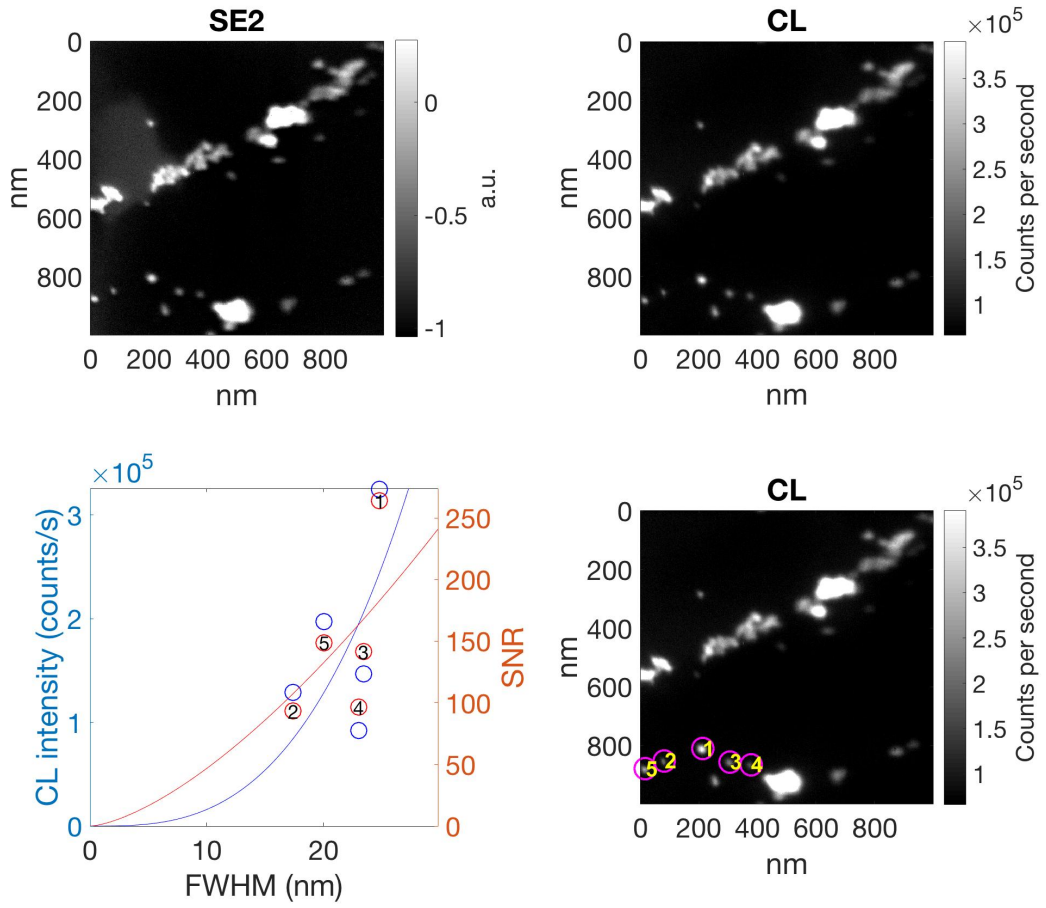

Figure S17. Raw SE2 and CL data for $NaGdF_4$:5% Eu^{3+} nanoparticles used for data points in Fig. 3a, Position 1 taken using a 5 keV electron beam, ~400 pA beam current, 2 ms dwell time, and a 512 x 512 pixel grid with 1.95 nm pixel pitch. The two CL images on the right are identical with the exception that the single nanoparticles that were analyzed are indexed in the bottom panel. CL Gaussian amplitude (left axis, blue circles) and the signal-to-noise ratio (CL SNR, right axis, red circles) are plotted as a function of nanoparticle size (SEM full-width-half-maximum, SEM FWHM) in the bottom-left panel. Each CL SNR data point is labeled with the nanoparticle index. CL intensity is fitted to a cubic curve, while the CL SNR is fitted to a power law with an exponent of 3/2.

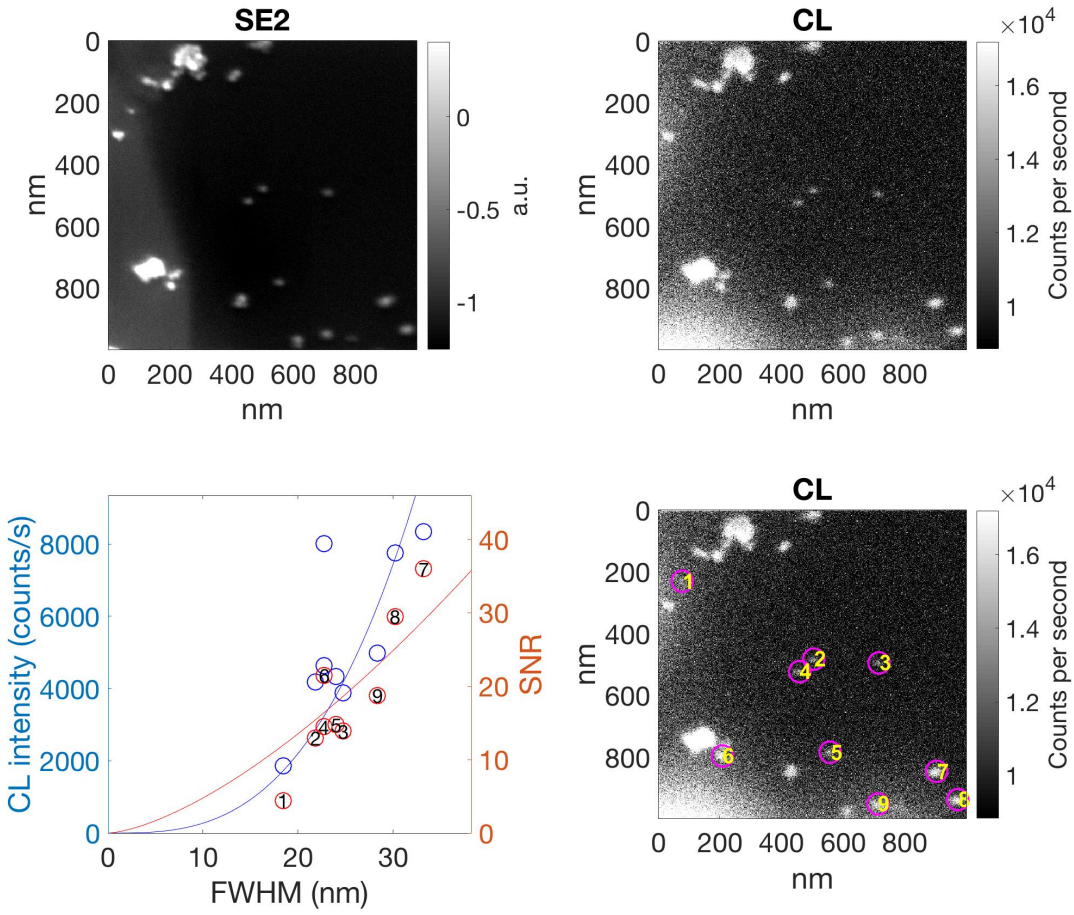

Figure S18. Raw SE2 and CL data for $NaGdF_4$:5% Eu^{3+} nanoparticles used for data points in Fig. 3a, Position 2 taken using a 5 keV electron beam, ~400 pA beam current, 2 ms dwell time, and a 512 x 512 pixel grid with 1.95 nm pixel pitch. The two CL images on the right are identical with the exception that the single nanoparticles that were analyzed are indexed in the bottom panel. CL Gaussian amplitude (left axis, blue circles) and the signal-to-noise ratio (CL SNR, right axis, red circles) are plotted as a function of nanoparticle size (SEM full-width-half-maximum, SEM FWHM) in the bottom-left panel. Each CL SNR data point is labeled with the nanoparticle index. CL intensity is fitted to a cubic curve, while the CL SNR is fitted to a power law with an exponent of 3/2.

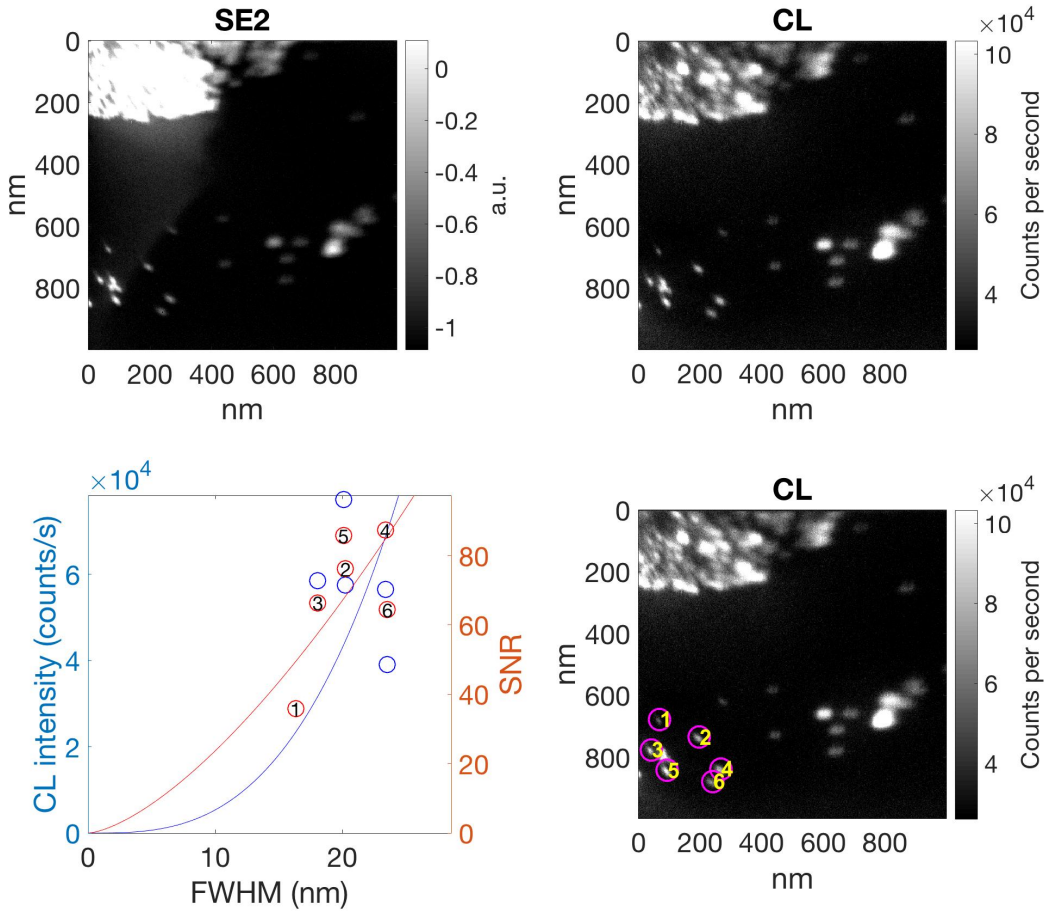

Figure S19. Raw SE2 and CL data for $NaGdF_4$:5% Eu^{3+} nanoparticles used for data points in Fig. 3a, Position 3 taken using a 5 keV electron beam, ~400 pA beam current, 2 ms dwell time, and a 512 x 512 pixel grid with 1.95 nm pixel pitch. The two CL images on the right are identical with the exception that the single nanoparticles that were analyzed are indexed in the bottom panel. CL Gaussian amplitude (left axis, blue circles) and the signal-to-noise ratio (CL SNR, right axis, red circles) are plotted as a function of nanoparticle size (SEM full-width-half-maximum, SEM FWHM) in the bottom-left panel. Each CL SNR data point is labeled with the nanoparticle index. CL intensity is fitted to a cubic curve, while the CL SNR is fitted to a power law with an exponent of 3/2.

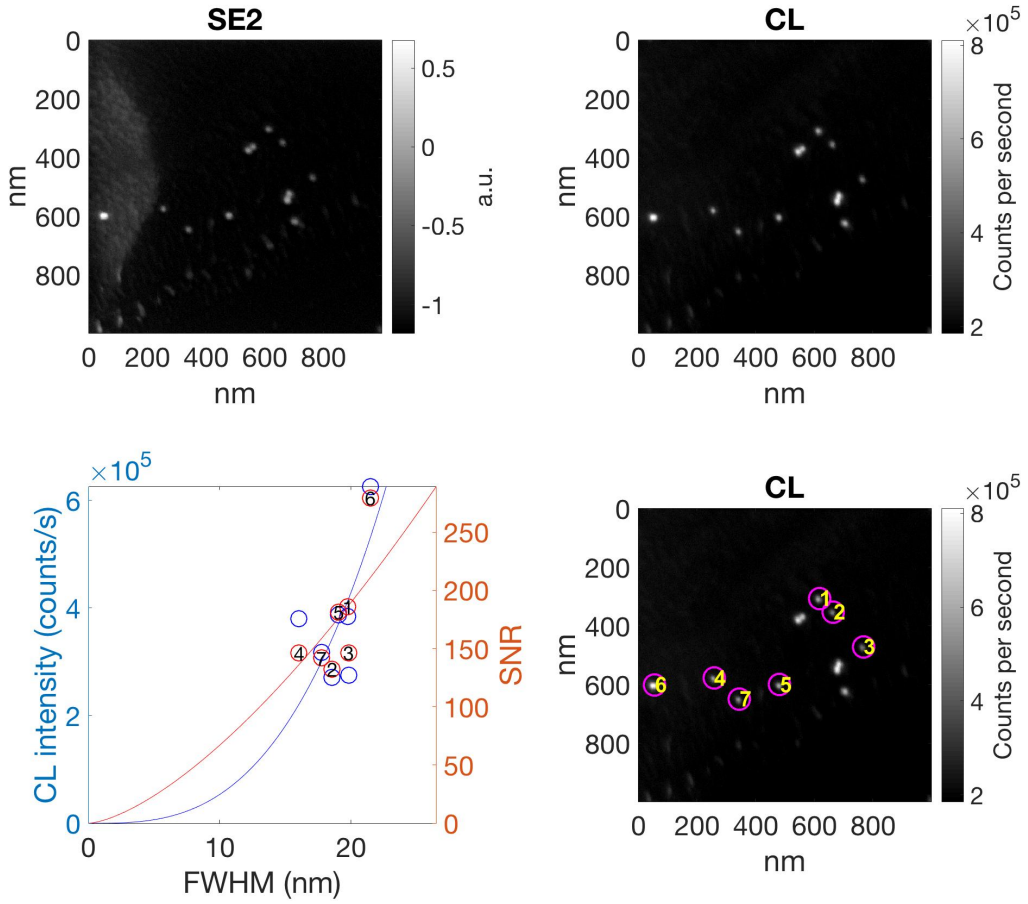

Figure S20. Raw SE2 and CL data for $NaGdF_4$:5% Eu^{3+} nanoparticles used for data points in Fig. 3a, Position 4 taken using a 5 keV electron beam, ~400 pA beam current, 2 ms dwell time, and a 512 x 512 pixel grid with 1.95 nm pixel pitch. The two CL images on the right are identical with the exception that the single nanoparticles that were analyzed are indexed in the bottom panel. CL Gaussian amplitude (left axis, blue circles) and the signal-to-noise ratio (CL SNR, right axis, red circles) are plotted as a function of nanoparticle size (SEM full-width-half-maximum, SEM FWHM) in the bottom-left panel. Each CL SNR data point is labeled with the nanoparticle index. CL intensity is fitted to a cubic curve, while the CL SNR is fitted to a power law with an exponent of 3/2.

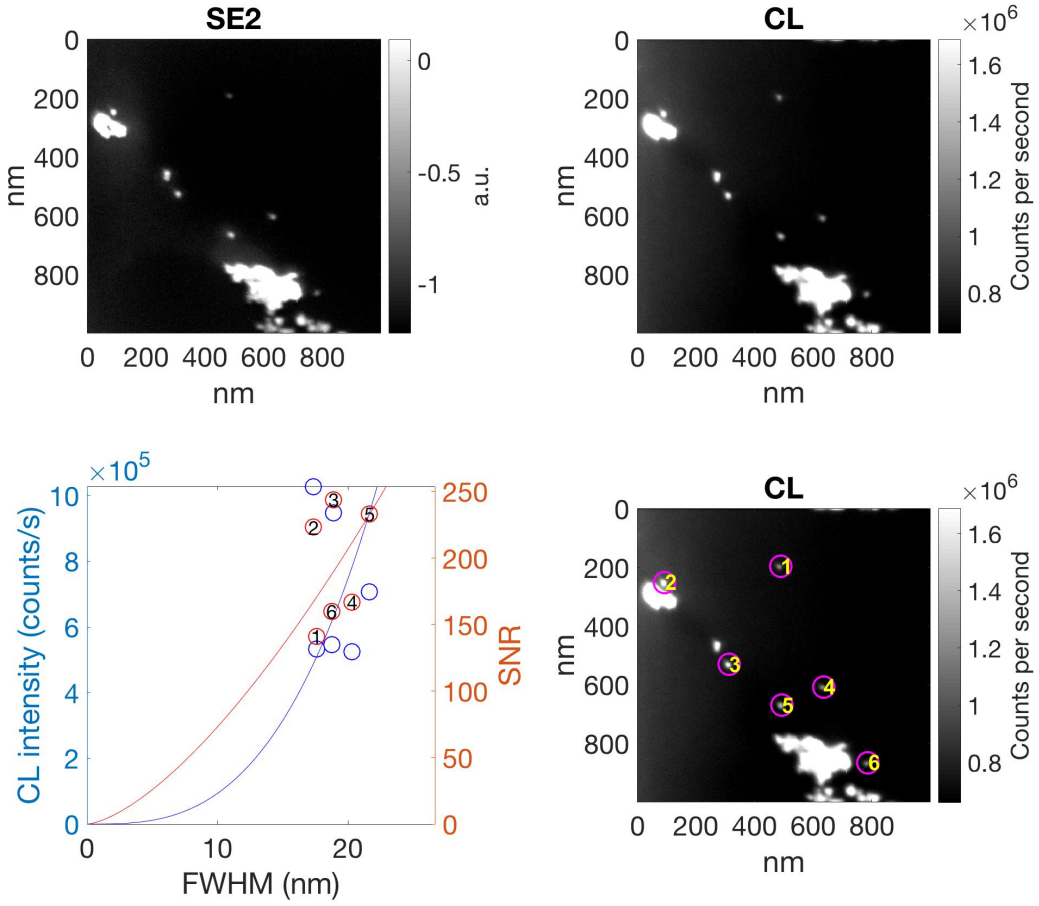

Figure S21. Raw SE2 and CL data for $NaGdF_4$:5% Eu^{3+} nanoparticles used for data points in Fig. 3a, Position 5 taken using a 5 keV electron beam, ~400 pA beam current, 2 ms dwell time, and a 512 x 512 pixel grid with 1.95 nm pixel pitch. The two CL images on the right are identical with the exception that the single nanoparticles that were analyzed are indexed in the bottom panel. CL Gaussian amplitude (left axis, blue circles) and the signal-to-noise ratio (CL SNR, right axis, red circles) are plotted as a function of nanoparticle size (SEM full-width-half-maximum, SEM FWHM) in the bottom-left panel. Each CL SNR data point is labeled with the nanoparticle index. CL intensity is fitted to a cubic curve, while the CL SNR is fitted to a power law with an exponent of 3/2.

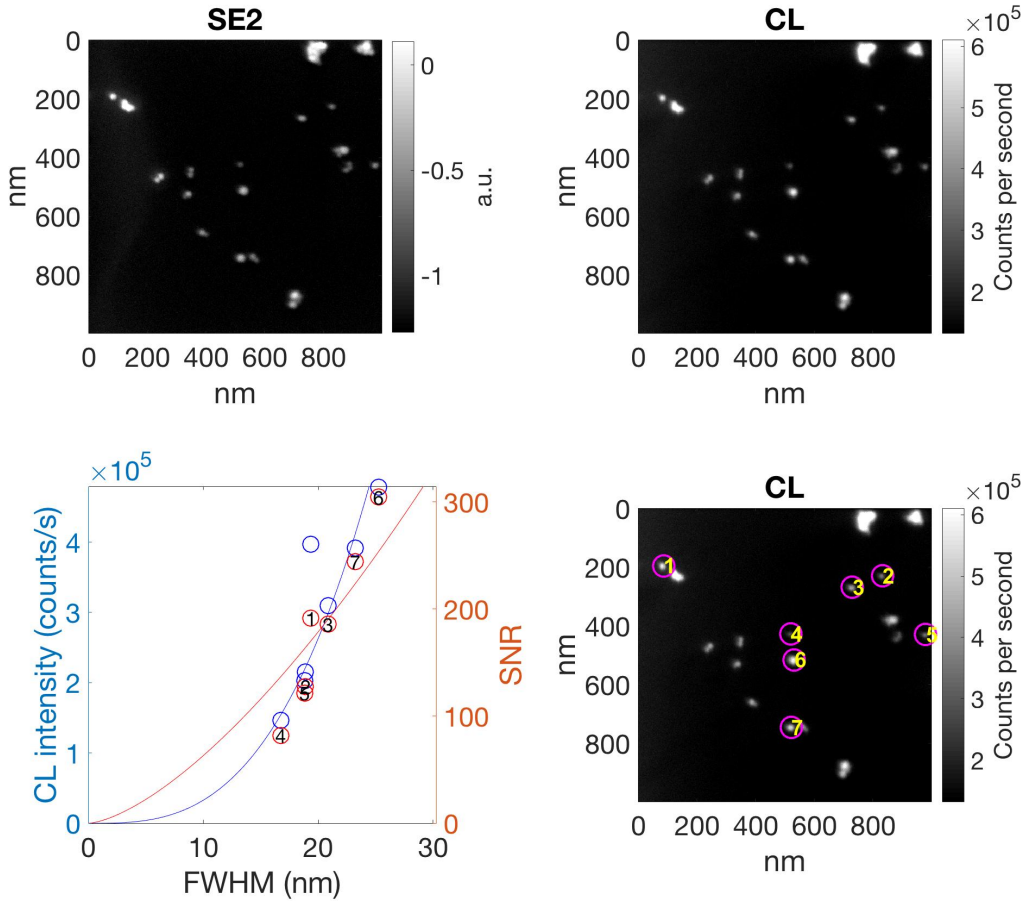

Figure S22. Raw SE2 and CL data for $NaGdF_4$:5% Eu^{3+} nanoparticles used for data points in Fig. 3a, Position 6 taken using a 5 keV electron beam, ~400 pA beam current, 2 ms dwell time, and a 512 x 512 pixel grid with 1.95 nm pixel pitch. The two CL images on the right are identical with the exception that the single nanoparticles that were analyzed are indexed in the bottom panel. CL Gaussian amplitude (left axis, blue circles) and the signal-to-noise ratio (CL SNR, right axis, red circles) are plotted as a function of nanoparticle size (SEM full-width-half-maximum, SEM FWHM) in the bottom-left panel. Each CL SNR data point is labeled with the nanoparticle index. CL intensity is fitted to a cubic curve, while the CL SNR is fitted to a power law with an exponent of 3/2.

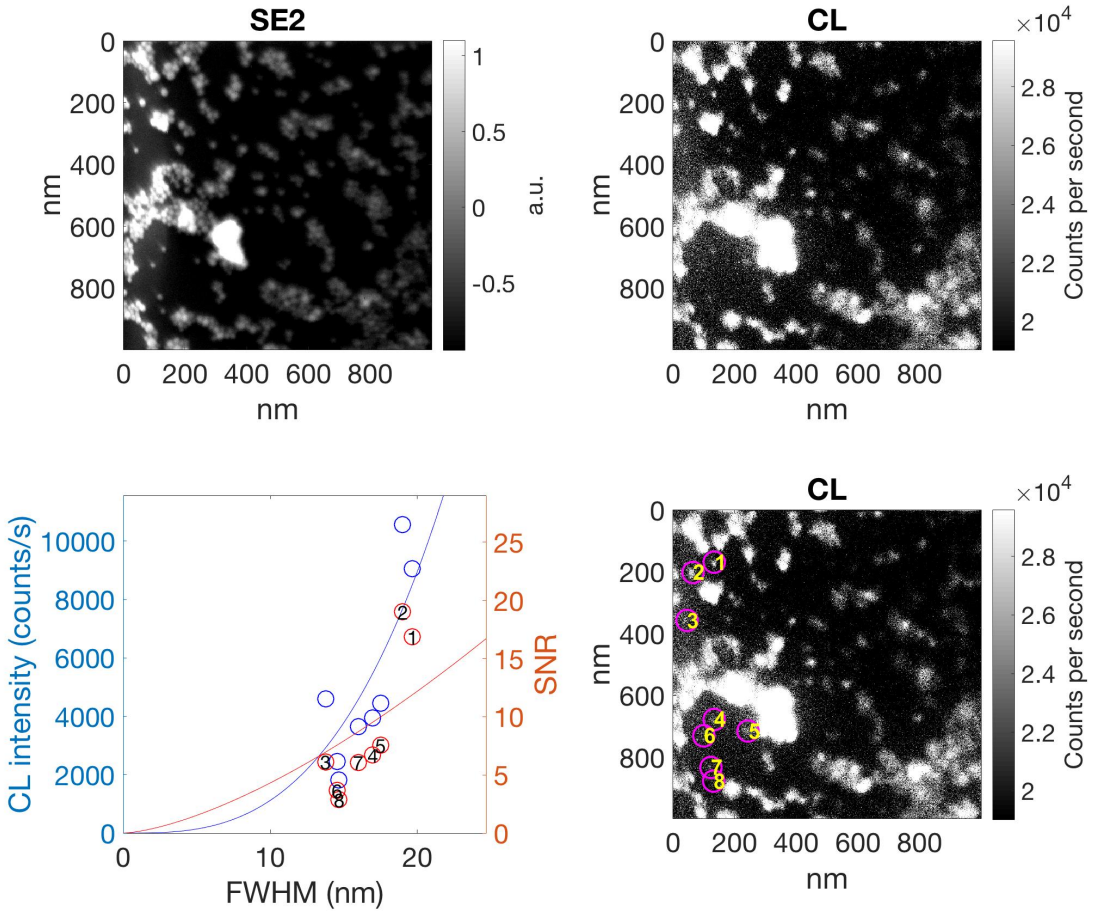

Figure S23. Raw SE2 and CL data for $NaGdF_4$:5% Eu^{3+} nanoparticles used for data points in Fig. 3a, Position 7 taken using a 5 keV electron beam, ~400 pA beam current, 2 ms dwell time, and a 512 x 512 pixel grid with 1.95 nm pixel pitch. The two CL images on the right are identical with the exception that the single nanoparticles that were analyzed are indexed in the bottom panel. CL Gaussian amplitude (left axis, blue circles) and the signal-to-noise ratio (CL SNR, right axis, red circles) are plotted as a function of nanoparticle size (SEM full-width-half-maximum, SEM FWHM) in the bottom-left panel. Each CL SNR data point is labeled with the nanoparticle index. CL intensity is fitted to a cubic curve, while the CL SNR is fitted to a power law with an exponent of 3/2.

Table S1. Absolute total number of $NaGdF_4$:5% Eu^{3+} nanoparticles observed in each sample shown in Main Text Fig. 3a-c, the absolute number of observed nanoparticles with CL SNR>10, and the percentage of nanoparticles with CL SNR>10. Note that every single $NaGdF_4$:5% Eu nanoparticle presented in Main Text Fig. 3 was detected in the SEM SE2 channel but not all the detected nanoparticles had the CL SNR>10.

Panel (a)								
Position	**1**	**2**	**3**	**4**	**5**	**6**	**7**	
Total # detected by SEM	5	9	6	7	6	7	8	
CL SNR>10	5	8	6	7	6	7	2	
% CL SNR>10	100	89	100	100	100	100	25	
Panel (b)								
Sample	**1**	**2**	**3**	**4**	**5**	**6**	**7**	**8**
Total # detected by SEM	17	5	7	21	27	31	39	18
CL SNR>10	17	5	7	21	26	14	38	4
% CL SNR>10	100	100	100	100	96	45	97	22
Panel (c)								
Synthesis	**1**	**2**	**3**	**4**	**5**	**6**	**7**	
Total # detected by SEM	17	40	18	14	13	4	18	
CL SNR>10	17	0	2	13	7	0	0	
% CL SNR>10	100	0	11	93	54	0	0	

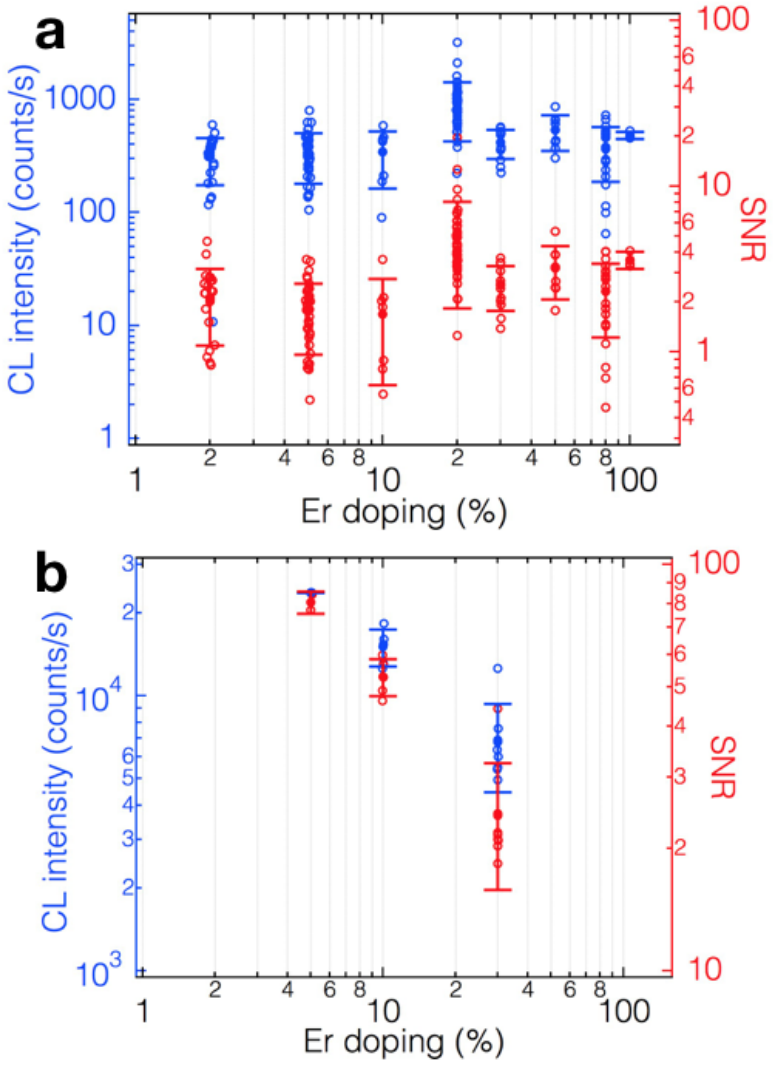

Figure S24. Single nanoparticle measurements of CL brightness as a function of Er^{3+} doping concentration for $NaGdF_4$ host (a) and $NaYF_4$ host (b). Each blue empty circle corresponds to a single nanoparticle within a 1 μm^2 field of view and represents the brightness (Gaussian amplitude) in counts per second (blue, y-axis on the left). Each red empty circle represents the signal-to-noise ratio for each nanoparticle (red, y-axis on the right). Filled circles represent the average brightness in counts per second (blue, y-axis on the left) and the CL signal-to-noise ratio (CL SNR, red, y-axis on the right). Error bars represent one standard deviation from the mean.

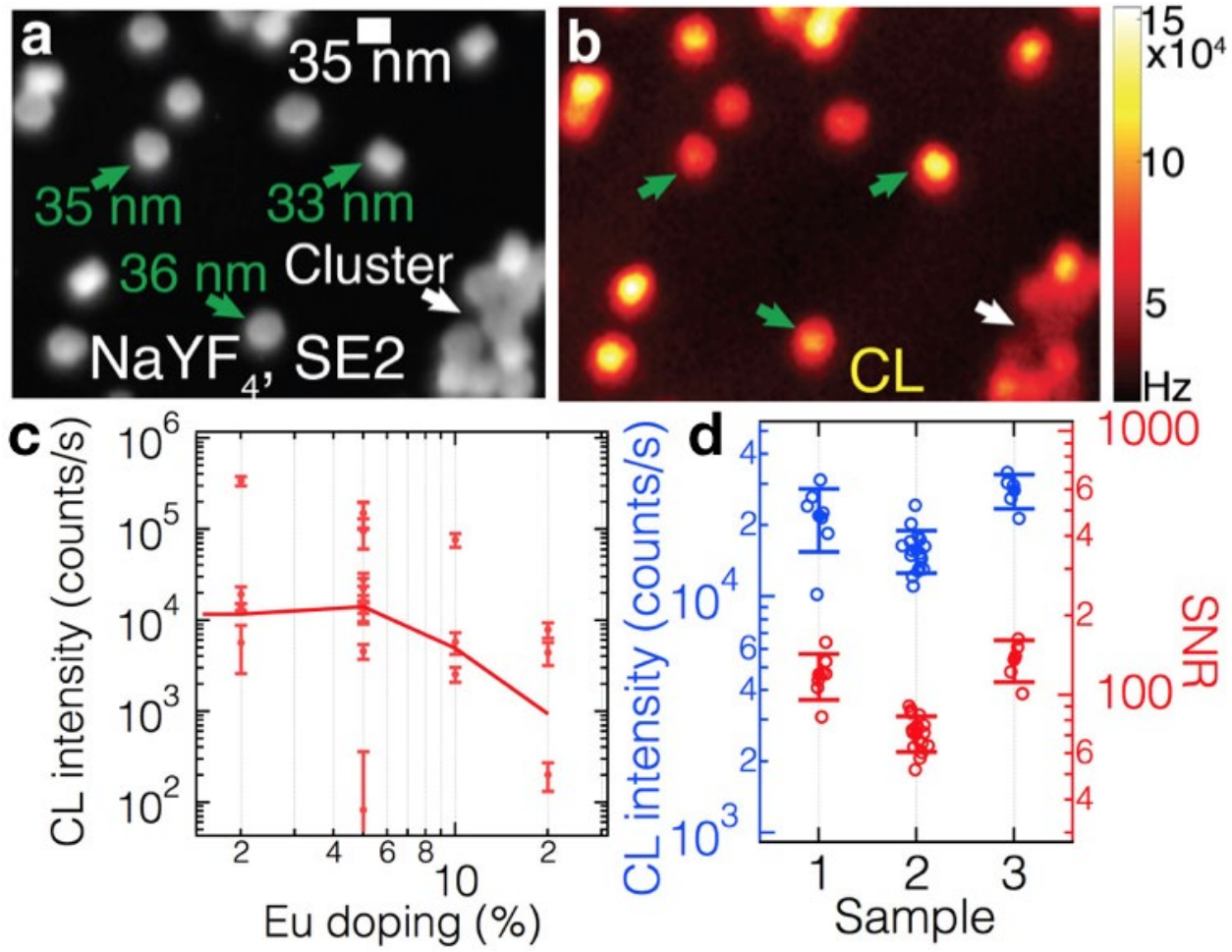

Figure S25. Single-nanoparticle CL measurements of BF_4^--exchanged $NaYF_4$:Eu^{3+} nanoparticles spin-coated on the Si substrate. Beam energy is 5 keV; beam current is ~400 pA; the original image was collected using a 512 x 512 pixel grid with a 1.95 nm pixel pitch. Secondary electron SE2 (a) and cathodoluminescence (b) images of $NaYF_4$:5% Eu^{3+} nanoparticles collected in parallel. The images in (a-b) are smoothed with a Gaussian filter with a standard deviation of 1.95 nm. Although some nanoparticles formed clusters (white arrows), only single non-clustered nanoparticles were used for the intensity analysis (green arrows). The SEM FWHM of several nanoparticles is shown in green. (c) Single nanoparticle measurements of CL brightness as a function of Eu^{3+} doping concentration for $NaYF_4$ host. Each data point corresponds to an average of nanoparticle brightness in a single 1 μm^2 field of view and the corresponding error bars show one standard deviation of the mean. All data are plotted including images from different syntheses, different samples from the same synthesis, and data from different regions of the same sample. Solid red line represents an average of the intensities of all measurements at each individual Eu^{3+} doping level. This figure is an equivalent of the Main Text Fig. 3d but for the $NaYF_4$ host. (d) Reproducibility of CL brightness in three separate $NaYF_4$:10% Eu^{3+} samples from the same synthesis run.

Ensemble spectral measurements and sample preparation:

For ensemble cathodoluminescence spectral measurements, the nanoparticle samples were washed three times by adding 0.5 mL of as-synthesized nanoparticle solution in oleic acid (Sigma-Aldrich, Cat# 364525-25ML, 90%, technical grade) and 1-octadecene (Sigma-Aldrich, Cat# O806-1L, 90%, technical grade) to 0.5 mL ethanol (Sigma-Aldrich, Cat# 459844-1L, ACS Reagent, >99.5%, 200 proof) in a 1.5 mL Eppendorf centrifuge tube (Eppendorf, safe-lock tubes, 1.5 mL, Cat# 022363204), centrifuging at 3.5 g for 3 minutes at room temperature, and re-dispersing the nanoparticles in *n*-hexane (Macron Fine Chemicals, Cat# H487-10, 95%). After the wash, the nanoparticles were drop-cast repeatedly on a ~5 mm x 5 mm piece of silicon wafer (Ted Pella, ultra-flat, 6", Cat# 21610-4, <100>, P/Boron-doped, 1-10 Ω/cm) by applying ~5-10 µL of nanoparticle suspension in *n*-hexane to the wafer and letting the solvent evaporate. The procedure was repeated until an opaque white film of nanoparticles was visible by eye on the surface of the silicon wafer.

Nanoparticle spectra were measured in the Microchemical Analysis Facility at Stanford University with a JEOL JXA-8230 SuperProbe electron microscope equipped with an xCLent III hyperspectral cathodoluminescence system. For each sample, the spectra were recorded at 900 points on a 30 x 30 square grid with a side of 180 µm. The pitch of the grid was equal to 6 µm. The resulting spectra were averaged to obtain the CL intensity. The current density in these experiments was ~0.13 pA/nm^2 (8,125 electrons s^{-1} Å^{-2}), which is ~1000 times lower than the current density used in the single-particle CL experiments (~100 pA/nm^2, 6.24 x 10^6 electrons s^{-1} Å^{-2}). In addition, the sample preparation was different between these two experiments (protocols described above). Such factors as the imaging conditions and the sample preparation influence the luminescence properties of nanoparticles as well as their susceptibility to electron beam damage. Ultimately, since the goal of the biological CL microscopy is to register the position and color of individual rare-earth nanoparticles, the single-nanoparticle CL measurements are more relevant for the purpose of this work than the ensemble measurements such as the ones shown in Fig. S26.

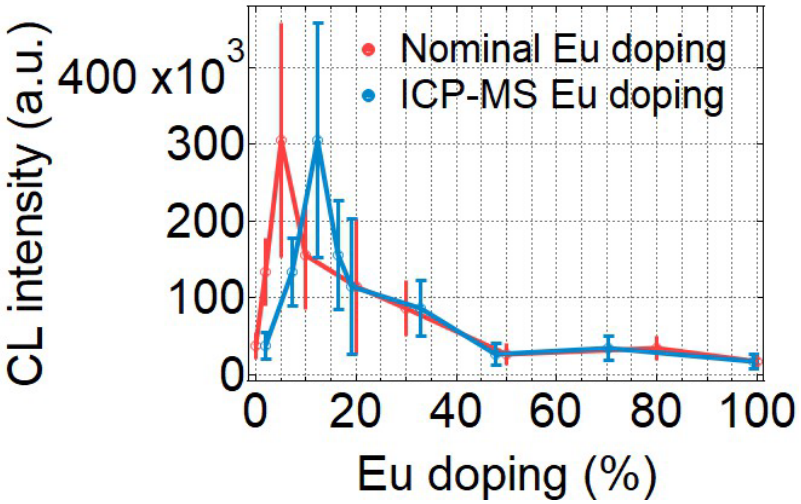

Figure S26. Ensemble CL emission from films of $NaGdF_4$ nanoparticles doped with various concentrations of Eu^{3+} and drop cast on a silicon substrate. Nominal Eu^{3+} doping is in red, Eu^{3+} doping determined by ICP-MS (Fig. S8) is in blue.

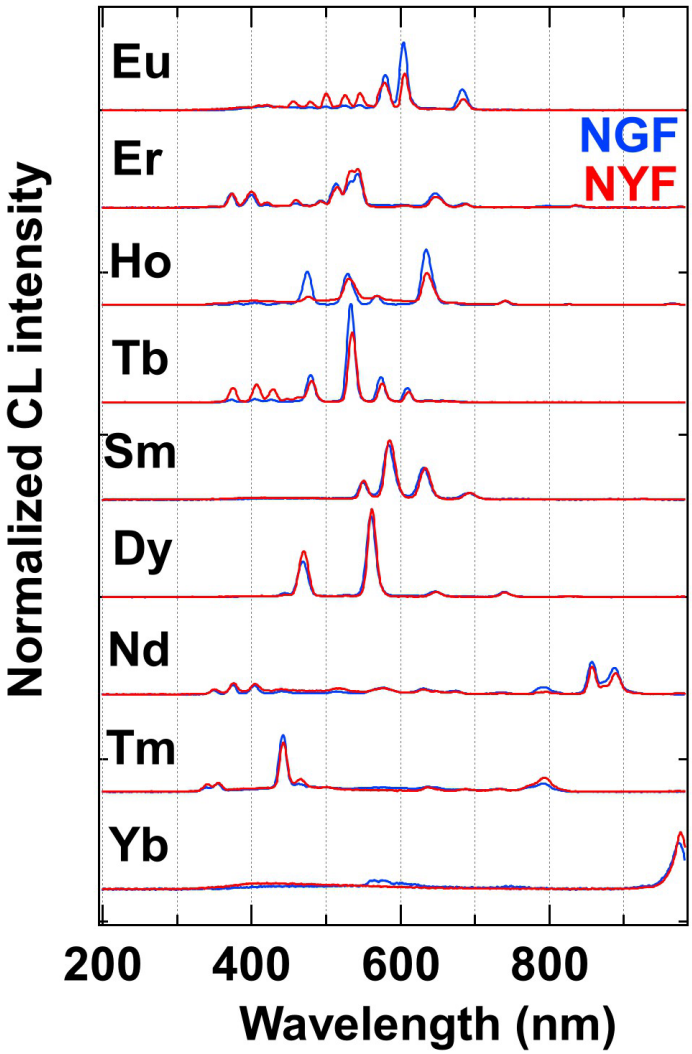

Figure S27. Comparison of ensemble nanoparticle spectra for $NaYF_4$ and $NaGdF_4$ host lattice. All $NaYF_4$ nanoparticles were doped at 5 %. All $NaGdF_4$ nanoparticles were doped at 15 % except Er^{3+}, which was doped at 20 %. NGF is $NaGdF_4$, spectra in blue; NYF is $NaYF_4$, spectra in red.

Estimation of the number of observable colors and the required photon count rate:

In this section we are concerned with the following problem: Assume that we observed a certain 'noisy' CL-spectrum for an individual nanoparticle. What is the minimum required photon number (S_{total}) that enables a correct determination of the dopant type?

To estimate the required S_{total} we combine the ensemble spectra shown in Fig. 4 of the main text with Monte Carlo simulations. For a given nanoparticle of S_{total} we can simulate the nanoparticle spectrum, including shot noise, as $\vec{S} = (S_{\lambda_1}, S_{\lambda_2}, , S_{\lambda_N})$, where $S_{\lambda_i} \sim Pois(s_{\lambda_i})$ denotes a random variable corresponding to the number of photons detected at a wavelength λ_i. The photon number s_{λ_i} represents the expected photon count from the ensemble spectrum at wavelength λ_i and adds up to a total detected photon number $S_{total} = \Sigma_i s_{\lambda_i}$. Fig. S28 shows simulated *random experiments* for three different instances of Tb-containing nanoparticles with a total $\langle \vec{S}_{total} \rangle = 5$, 20 and 100 (red), and the ensemble spectrum (blue). To determine what lanthanide dopant is most likely resulting in the simulated spectrum we calculate the correlation coefficient

$\rho(\vec{S}, \vec{S}^X_{exp}) = \vec{S} \cdot \vec{S}^X_{exp}/(|\vec{S}||\vec{S}^X_{exp}|)$ between the detected spectrum $\vec{S}$ and the ensemble spectrum $\vec{S}^X_{exp}$ for each lanthanide dopant X. The spectrum is then assigned to the lanthanide ion with the largest correlation coefficient. Fig. S28 depicts the simulated probability (N = 5,000) of incorrectly assigning the ion type for variable $\vec{S}_{total}$ and different lanthanide dopants. For a photon count of 21 counts, the probability of correctly assigning a given spectrum to an arbitrary lanthanide ion exceeds 95%. Note that this is comparable to our typical count rates of 10,000 cps and a pixel dwell time of 2 ms.

It is worth noting that in this analysis we assume a spectral resolution exceeding 1 nm. However, in a real experiment an APD or PMT array would most likely be used. Different colors would then be separated by a combination of dichroic and band-pass filters. Such a configuration will significantly reduce resolution, and likely be limited to less than ten wavelengths. Furthermore, we assumed that the CL spectrum of individual nanoparticles is identical to that of ensemble samples, which needs to be experimentally confirmed. Further investigation on the spectral properties and CL intensity of individual nanoparticles needs to be performed.

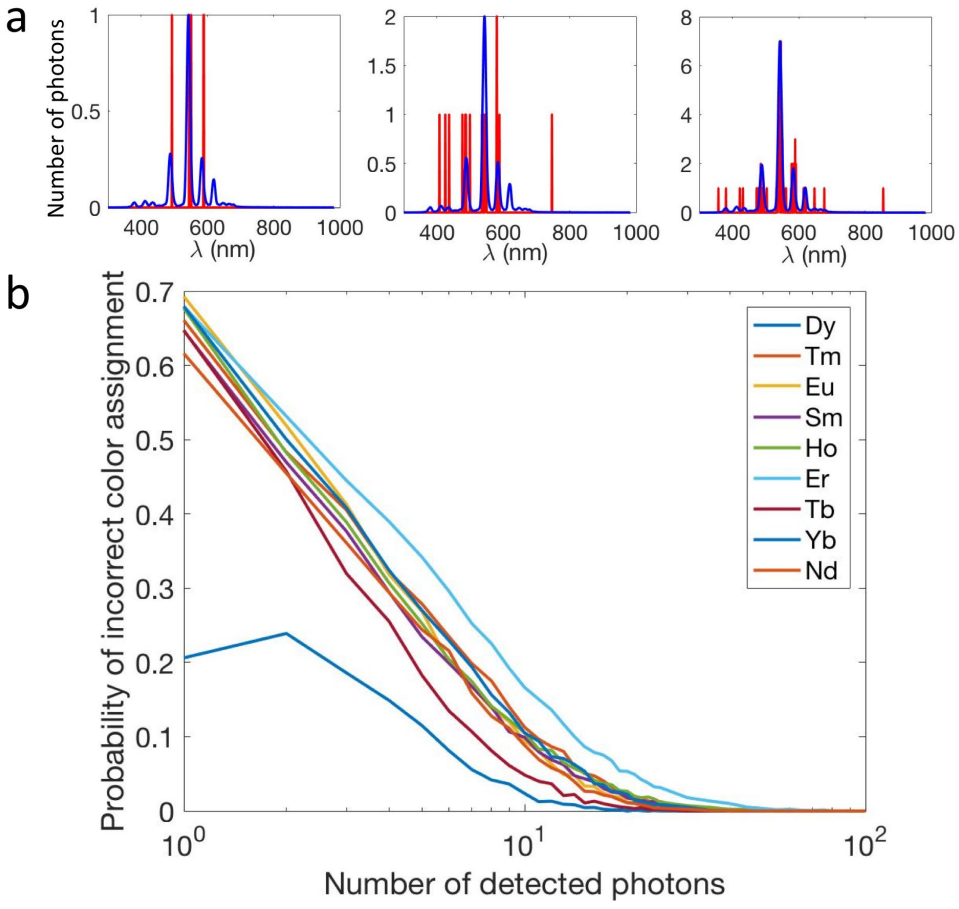

Figure S28. (a) Ensemble spectrum of Tb^{3+} and a *random experiment* for an average of 5, 20 and 100 detected photons. (b) Simulation probability for incorrectly assigning the lanthanide dopant type (see legend for color code) as a function of the number of detected photons.

Ensemble lifetime measurements:

The sample for ensemble lifetime measurements was prepared using a similar procedure to the one used for single-nanoparticle sample preparation with an exception that more material was used to achieve a larger amount of sample on the Si wafer.

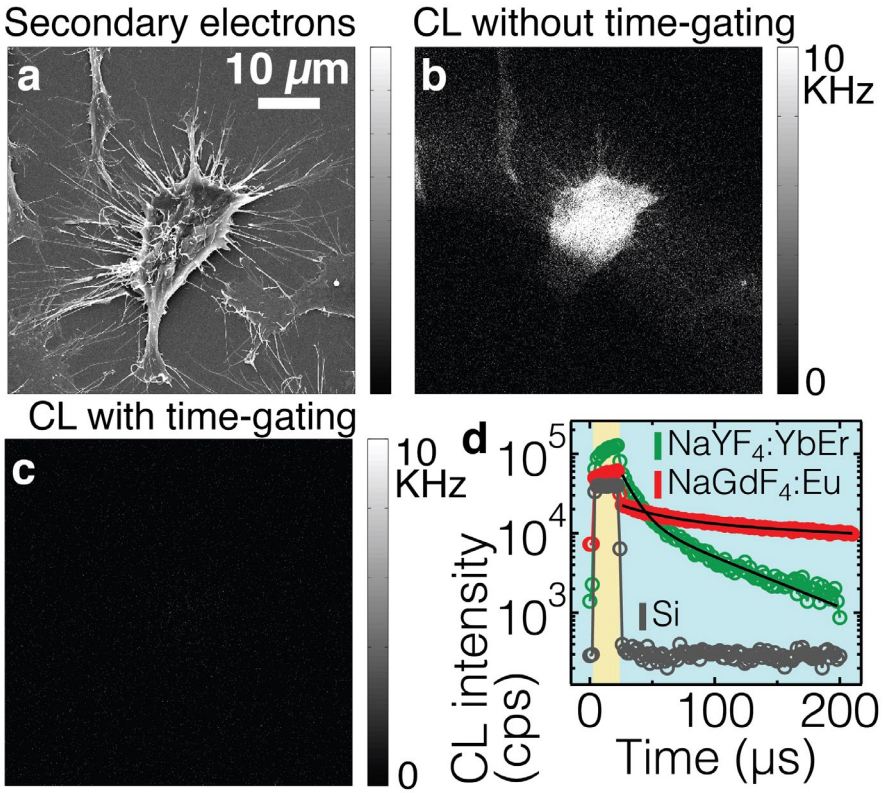

Figure S29. Lifetimes and time-gating of rare-earth nanoprobes. A HeLa cell imaged with secondary electrons (a) and in cathodoluminescence without (b) and with (c) time-gating. The wait time between when the electron beam was turned off and when the CL detection began was 1 μs. Time-gating eliminated background fluorescence, resulting in the absence of signal in panel (c) as compared to panel (b). (d) The CL lifetimes of two types of rare-earth nanoparticles are long-lived compared to the Si substrate. Yellow background indicates that the electron beam is on, blue – electron beam is off. $NaYF_4$ nanoparticles were doped with 18 % Er, and 2 % Er. $NaGdF_4$ nanoparticles were doped with 20 % Eu.

Spectra for Ce^{3+}, Pr^{3+} and Gd^{3+}:

Figure S29 shows the CL spectra obtained for nanoparticles doped with Gd^{3+}, Ce^{3+}, and Pr^{3+}. While Pr^{3+} consists of several sharp lines (indicating 4*f*-to-4*f* transitions) with a broad background, neither Ce^{3+} nor Gd^{3+} showed any narrow spectral features. The broad spectra likely originate from processes not associated to electronic transitions in lanthanide ions.

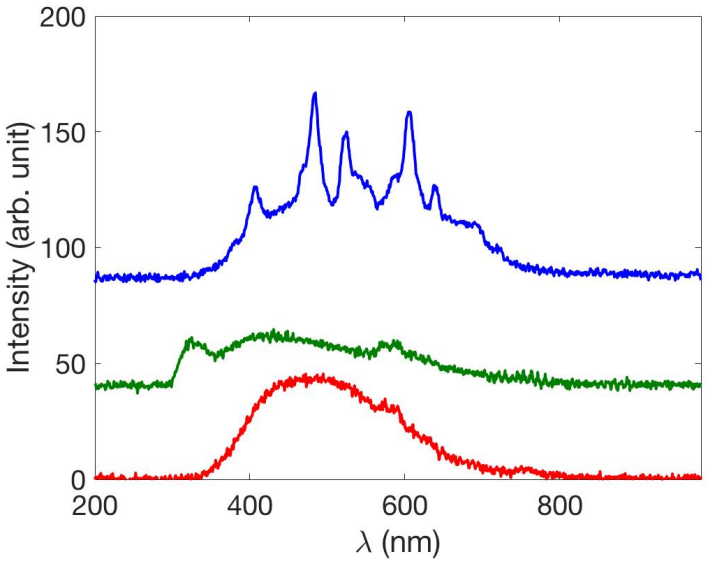

Figure S30. CL signal of a film of Gd^{3+} (red), Ce^{3+} (green) and Pr^{3+} (blue). Broad spectral features may originate from organic impurities.

Simulations of nanoparticle spectra

Fig. S31 shows the energy level diagram and the simulated (non-)radiative transition rates for Er^{3+} (right) and Eu^{3+} (left) ions. In practice, the highest available energy level in our software package[10] is populated by applying a resonant field (red upward-pointing arrow at a simulated intensity of 10 kW/cm^2; excitation wavelength for Er^{3+}: 195nm, Eu^{3+}: 351nm. Simulations for the remaining ions (not shown) used the following excitation wavelength Sm^{3+}: 415nm, Ho^{3+}: 277nm, Tm^{3+}: 358nm, Tb^{3+}: 373nm, Dy^{3+}: 364nm, Nd^{3+}: 355nm, Yb^{3+}: 980nm). After 1.6 ms of simulation time, a steady state was achieved, and the individual radiative transition rates were obtained (red and green downward-pointing arrows).

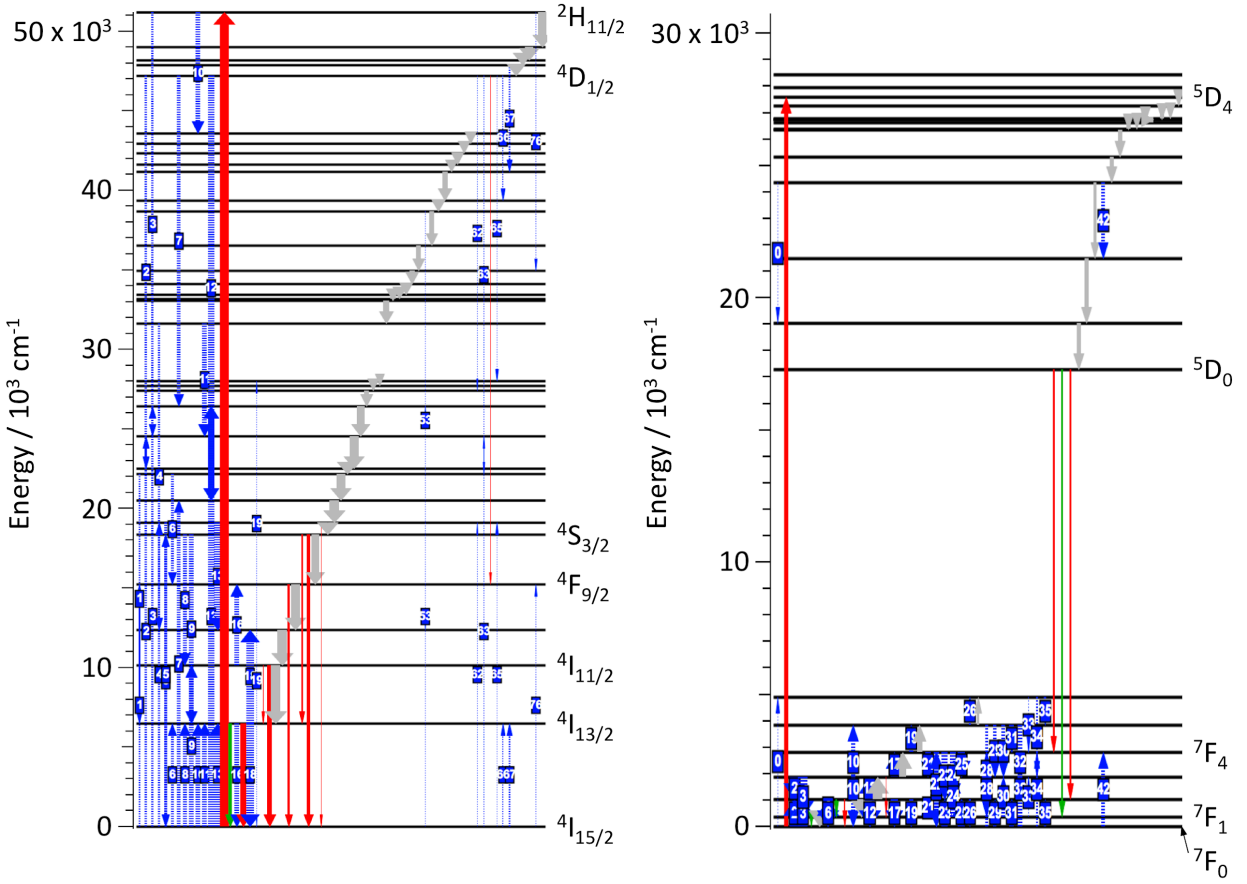

Figure S31. Representative example of simulated energy level diagram for Er^{3+} (right) and Eu^{3+} (left) ions with 20 % doping density. The arrows thicknesses are proportional to the transition rates. Red arrows correspond to electric dipole transitions, green – to magnetic dipole transitions, blue – to resonant energy transfer between ions, and grey – to phonon-induced relaxations.

References

1. Wang, F., Deng, R. & Liu, X. Preparation of core-shell NaGdF4 nanoparticles doped with luminescent lanthanide ions to be used as upconversion-based probes. *Nat. Protoc.* **9,** 1634–1644 (2014).
2. Liu, Q., Feng, W., Yang, T., Yi, T. & Li, F. Upconversion luminescence imaging of cells and small animals. *Nat. Protoc.* **8,** 2033–2044 (2013).
3. Li, Z. & Zhang, Y. An efficient and user-friendly method for the synthesis of hexagonal-phase NaYF4:Yb, Er/Tm nanocrystals with controllable shape and upconversion fluorescence. *Nanotechnology* **19,** 345606 (2008).

4. Ostrowski, A. D. *et al.* Controlled synthesis and single-particle imaging of bright, sub-10 nm lanthanide-doped upconverting nanocrystals. *ACS Nano* **6,** 2686–2692 (2012).
5. Durham, D. B., Frank Ogletree, D. & Barnard, E. S. Scanning Auger spectromicroscopy using the ScopeFoundry software platform. *Surf. Interface Anal.* (2018).
6. Dong, A. *et al.* A generalized ligand-exchange strategy enabling sequential surface functionalization of colloidal nanocrystals. *J. Am. Chem. Soc.* **133,** 998–1006 (2011).
7. Berger, M. J. & Seltzer, S. M. *Tables of Energy Losses and Ranges of Electrons and Positrons*. (1964).
8. Joy, D. C. & Luo, S. An empirical stopping power relationship for low-energy electrons. *Scanning* **11,** 176–180 (1989).
9. Kanaya, K. & Okayama, S. Penetration and energy-loss theory of electrons in solid targets. *J. Phys. D Appl. Phys.* **5,** 43–58 (1972).
10. Chan, E. M. Combinatorial approaches for developing upconverting nanomaterials: high-throughput screening, modeling, and applications. *Chem. Soc. Rev.* **44,** 1653–1679 (2015).